Biology of Reproduction, 2024, **110(4)**, 782–797
https://doi.org/10.1093/biolre/ioae010
Advance access publication date 15 January 2024
Research Article

Targeted deletion of NR2F2 and VCAM1 in theca cells impacts ovarian follicular development: insights into polycystic ovary syndrome?†

Nicholes R. Candelaria and JoAnne S. Richards*

Department of Molecular & Cellular Biology, Baylor College of Medicine, Houston, TX, USA
***Correspondence:** Department of Molecular & Cellular Biology, Baylor College of Medicine, 1 Baylor Plaza, Houston, TX 77030, USA. Tel: 1 (832) 421-3916; E-mail: joanner@bcm.edu

†**Grant Support:** This work was supported by the National Institutes of Health, NIH-HD-076980 (JSR) and by the Integrated Microscopy Core with funding from the Dan L Duncan Cancer Center, the Gulf Coast Consortium for Chemical Genomics, and the Pathology and Histology Core at Baylor College of Medicine (DK56338 and Ca125123).

Abstract

Defining features of polycystic ovary syndrome (PCOS) include elevated expression of steroidogenic genes, theca cell androgen biosynthesis, and peripheral levels of androgens. In previous studies, we identified vascular cell adhesion molecule 1 (VCAM1) as a selective androgen target gene in specific NR2F2/SF1 (+/+) theca cells. By deleting NR2F2 and VCAM1 selectively in CYP17A1 theca cells in mice, we documented that NR2F2 and VCAM1 impact distinct and sometimes opposing theca cell functions that alter ovarian follicular development in vivo: including major changes in ovarian morphology, steroidogenesis, gene expression profiles, immunolocalization images (NR5A1, CYP11A1, NOTCH1, CYP17A1, INSL3, VCAM1, NR2F2) as well as granulosa cell functions. We propose that theca cells impact follicle integrity by regulating androgen production and action, as well as granulosa cell differentiation/luteinization in response to androgens and gonadotropins that may underlie PCOS.

Graphical Abstract

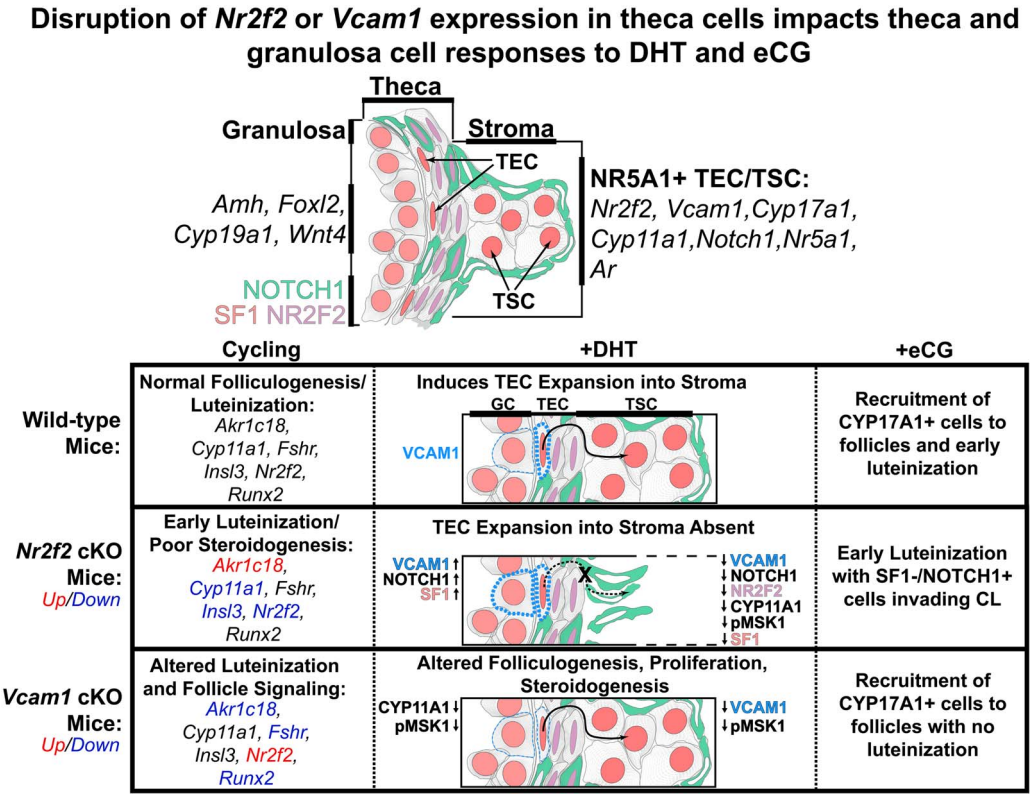

Key words: theca cells, NR2F2, VCAM1, CYP17A1, CYP11A1, NR5A1, NOTCH1, PCOS

Received: July 12, 2023. **Revised:** November 16, 2023. **Accepted:** January 10, 2024

Introduction

Polycystic ovary syndrome (PCOS) is a common anovulatory endocrine disorder in women [1–6]. It is associated with (1) elevated peripheral levels of luteinizing hormone (LH) and androgens indicative of altered theca cell functions, and (2) restricted follicular development with the absence of preovulatory follicles. Ovulation can be stimulated in many PCOS patients with exogenous gonadotropins (follicle-stimulating hormone (FSH)/luteinizing hormone (LH)), indicating that some follicles within the ovaries respond to exogenous hormone treatments [3].

Regulation of androgen biosynthesis in theca cells is tightly controlled not only by the pituitary LH but also by theca cell regulatory factors: steroidogenic factor 1 (SF1/*Nr5a1*) [7–11], the nuclear steroid co-regulatory factor COUPTF-II (NR2F2) [12–14], insulin-like 3 (INSL3) [12, 15–18] that is elevated in PCOS patients [19], and NR4A1 [20–22] that interacts to control the expression of CYP11A1 and CYP17A1, two essential steroidogenic enzymes [23]. Androgen biosynthesis is also regulated by estradiol via the estrogen receptor α (ESR1: ERα) present in theca cells [16, 23, 24]. Of note, genetic variants of NR2F2, NR4A1, AR, INSL3, and VCAM1 have been detected in the genome of PCOS patients [16, 21, 22, 25, 26]. Furthermore, recent studies have documented that theca cells not only produce androgens but also express the androgen receptor (AR; NR3C4), making theca cells [25], as well as granulosa cells [25], a target tissue of androgen action within the human ovary. Seminal studies by Sheng Wu et al.[27] showed that disruption of AR expression selectively in theca cells of mice (using *AR* fl/fl and *Cyp17a1*-iCre mice) prevented elevated exogenous androgens from inducing a PCOS-like ovarian phenotype. These observations indicated that altered theca cell functions and expression of AR were likely a primary cause of abnormal androgen production and action in theca cells of PCOS patients. Furthermore, theca cells obtained from ovaries of PCOS patients express elevated levels of steroidogenic genes compared to theca of control women and are more highly responsive to LH stimulation of androgen biosynthesis [25].

Our recent studies have confirmed specific expression of AR in granulosa, theca as well as stromal cells in the mouse ovary [25]. We have also shown that elevating androgen levels in mice with slow-release DHT pellets (dihydrotestosterone) alters ovarian follicular morphology and expression of genes in theca cells as well as granulosa cells [25]. Specifically, we have shown for the first time that DHT treatment of immature female mice increased theca cell-specific expression of vascular cell adhesion molecule 1 (VCAM1) and promoted the expansion of theca cells also expressing NR2F2 into the ovarian stromal compartment. Selective disruption of AR in theca cells of mice prevented the markedly induced expression of VCAM1, providing evidence that VCAM1 was an androgen-regulated gene in these cells and might underlie altered theca cell functions in women with PCOS. VCAM1 is a known marker of steroidogenic Leydig cells in the mouse testis, indicating that VCAM1 likely plays a key role in these steroidogenic cells and in male gonadal functions as well [25].

VCAM1 has been shown to impact many different physiological processes: immune cell attachment to vascular cells [28], neuronal precursor cell attachment to the stem cell niche [29], and attachment of embryonic cells to the allantoic placental membrane [30]. However, the function(s) of VCAM1 in the ovary and testis have not been clearly defined. NR2F2 is known to be a repressor/regulator of steroid receptor functions, including AR in other tissues [31, 32]. In the ovary, NR2F2 is expressed not only in the AR+ steroidogenic theca cells but also in the surrounding fibroblastic stroma. NR2F2 is not expressed in granulosa cells [25]. Although NR2F2 impacts endocrine tissue differentiation and development and is known to interact with steroid hormone receptors, the specific role(s) of NR2F2 in AR+SF1+ theca cell functions and steroidogenesis and its relation to VCAM1 have not been clearly defined during ovarian follicular development. Therefore, to determine the effects of NR2F2 and VCAM1 selectively in steroidogenic SF1+ theca cells of developing follicles (as opposed to NR2F2+ stromal cells) and their potential impact on ovulation, we have generated mice in which *Nr2f2* and *Vcam1* gene expression has been selectively disrupted using *Nr2f2 fl/fl* mice [33] and *Vcam1 fl/fl* mice [34] mated to *Cyp17a1*-iCre mice [35]. Exposure of these mice to exogenous androgen or gonadotropins revealed distinct changes in follicular development and ovulation.

Using theca cells derived from control and PCOS patients, we previously demonstrated regulatory functions of NR2F2 and VCAM1 on steroidogenic outcomes [36]. Collectively, results of these studies provide evidence that NR2F2 and VCAM1 impact distinct, sometimes opposing, theca cell functions that regulate ovarian follicular development *in vivo*, and cause major changes in ovarian morphology, granulosa cell functions, and steroidogenesis. We propose that theca cells impact follicle integrity by regulating androgen production and action, as well as granulosa cell differentiation/luteinization in response to gonadotropins.

Materials and methods

Animal studies

Mouse colonies were maintained in the Transgenic Mouse Facility as part of Baylor College of Medicine's (BCM) Center for Comparative Medicine, in accordance with guidelines outlined in *Guide for the Care and Use of Laboratory Animals*. The Animal Care and Use Committee at BCM approved experimental strategies performed in this manuscript. Mice were fed ad libitum and were maintained in a 16-h/8-h dark cycle.

Mouse lines

To generate *Vcam1* and *Nr2f2* cKO lines, *Vcam1 f/f* (B6.129(C3)-*Vcam1*^{tm2Flv}/J, The Jackson Laboratory, Bar Harbor, ME) and *Nr2f2 f/f* (Nr2f2$^{tm2.1Tsa}$) mice were mated to the *Cyp17a1*-iCRE mouse line Tg(*Cyp17a1*-iCRE)AJako provided by Chemyong Ko. *Vcam1 f/f Cyp17a1*-iCRE and *Nr2f2 f/f Cyp17a1*-iCRE mice were referred to as *Vcam1* cKO and *Nr2f2* cKO mice, respectively. LHCGR-HA mice were obtained from Laurinda Jaffe's laboratory to localize its expression in the ovary following treatments [37]. Wild-type (WT) C57BL/6 mice and CRE− littermates were used to control for the cKO condition in forthcoming comparisons. Floxed alleles and iCRE were detected in genomic samples by quantitative PCR experiments carried out by Transnetyx (Cordova, TN, USA).

Surgical procedures and treatments

Slow-release DHT pellets (60 days, 12.5 mg/pellet; Innovative Research of America, Sarasota, FL) were inserted subcutaneously into prepubertal WT, *Vcam1* cKO, *Nr2f2* cKO, and HA-LHCGR females. For these studies, DHT-treated females were collected after 1 week of treatment. Prepubertal female WT and cKO mice were injected IP with gonadotropins equine chorionic gonadotropin (eCG, 5 IU, 48 h) and human chorionic gonadotropin (hCG, 5 IU, 24 h) and were collected thereafter (Sigma-Aldrich).

Serum hormone measurements

Serum was isolated from prepubertal D25, 2 mo. pubertal AMC, *Vcam1* cKO, and *Nr2f2* cKO females in Microtainer Serum Separator Tubes (Beckton, Dickinson and Company, Franklin Lakes, NJ, USA). Serum hormone measurements were carried out by The University of Virginia Center for Research in Reproduction Ligand Assay and Analysis Core, supported by P50-HD28934 from Eunice Kennedy Shriver NICHD/NIH (NCTRI).

Gene expression analysis

To obtain total RNA from ovary and testis for downstream transcript analysis, we first isolated the organs in 1 mL of TRIzol Reagent (Thermo Fisher Scientific, Waltham, MA, USA). Chloroform and spinning allowed for the isolation of the aqueous phase. Then, 1:1 vol/vol 100% ethanol was added to precipitate RNA. This mixture is then applied to RNAeasy columns (Qiagen, Germantown, MD, USA) where the manufacturer's instructions for RNA cleanup were followed. Purified RNA was primed with OligoDT and reverse transcribed using the M-MLV Reverse Transcription System (Invitrogen, Carlsbad, CA) according to the manufacturer's protocol. Transcripts were amplified on the Rotor-Gene 6000 Thermocycler with transcript specific oligos obtained from Sigma-Aldrich, St. Louis, MO and are listed in Supplementary Table S1.

Immunofluorescence and microscopy

Tissue sample preparation

Isolated ovary and testis samples were fixed in 4% paraformaldehyde in phosphate-buffered saline (PBS) for 24 h. Following fixation, samples were transferred into 70% ethanol. Tissue processing and paraffin embedding were carried out by the Human Tissue Acquisition and Pathology Core at Baylor College of Medicine. These were sectioned to a thickness of 7 μm and applied to Superfrost Plus Micro Slides (VWR, Radnor, PA).

Immunofluorescence, antibodies, and additional stains

Wax-embedded tissue was cleared using five xylene washes, followed by 100% ethanol, 100% methanol, 70% ethanol, then by PBS. Antigen retrieval in sodium citrate buffer (pH = 6.5) for 25 min at 95°C was followed by a PBS wash. Individual sections were circled using the SuperHT Pap Pen (VWR). To block non-specific antigens, we incubated sections in 10% normal donkey serum (NDS; Invitrogen) dissolved in 0.1% Tween-20 in PBS for 30 min. Sections were washed several times in PBS. Antibodies were then dissolved in 0.1% NDS/0.05% Tween-20/PBS solution overnight at 4°C. Sections are washed several times in PBS to remove unbound antibody. Secondary antibodies (Invitrogen) were then applied to the tissue sections in 0.1% NDS/0.05% Tween-20/PBS solution for 30 min at room temperature. Slides were washed three times. To quench autofluorescence in tissue, 0.25% Sudan Black in 70% ethanol was applied to the tissue sections for 20 min. Sections are then washed to remove Sudan Black precipitate, then mounted in Aqua-Poly/Mount (Polysciences, Warrington, PA, USA). Representative hematoxylin and eosin (H&E) images were generated by sectioning blocks and dewaxing as described above until the sections are in aqueous PBS. This was followed by separate H&E exposures to generate representative H&E stained tissues, which were then dehydrated and mounted in Permount solution (Thermo Fisher Scientific). Antibodies used are as follows: αSMA [Sigma-Aldrich (AB_262054)], 20αHSD [Gift from Carlos Stocco (University of Illinois, Chicago, IL, USA)], AR [Santa Cruz Biotechnology (AB_1563391)], CD45 [BD Biosciences (AB_2174426)], CYP11A1 [gift from Dagmar Wilhelm (University of Queensland, Brisbane, Australia)], CYP17A1 [gift from Dr. Alan J. Conley (AB_2491005)], HA [Cell Signaling Technology (AB_1549585)], INSL3 [Invitrogen (AB_2642736)], pMSK1-Thr581 [Cell Signaling Technology (AB_2181783)], NOTCH1 [Cell Signaling Technology (AB_2153354)], NOTCH2 [Cell Signaling Technology (AB_10693319)], NR2F2 [Perseus Proteomics, Meguro, Tokyo, Japan (AB_2155627)], SF1 [gift from Kenichirou Morohashi, Kyushu University, Fukuoka, Japan], and VCAM1 [Abcam (AB_2721053)].

Microscopy and image preparation

Imaging instruments and support were provided by the BCM Integrated Microscopy Core. For immunofluorescence, imaging was performed on a Cytiva DVLive epifluorescence image restoration microscope using Olympus objectives (UPlanSApo 20×/0.75, PlanApo 40×/0.95, and UPlanSApo 100×/1.4) and a 1.9kx1.9x sCMOS camera. Z-Stacks (0.25 μm for the 100× objective) covering the whole nucleus (~10 μm) were acquired before applying a conservative restorative algorithm for quantitative image deconvolution. A projected image (maximum signal) from each Z-stack was generated in ImageJ2 (v2.3.0/1.53f), where it was pseudo-colored according to a linear RGB scale. Channels were layered using Adobe Photoshop Creative Cloud 2022 software. For images requiring a larger sample area, fluorescently labeled sections were imaged and stitched on a Biotek Cytation 5 at 20× magnification. Permanent H&E slides were imaged on a Nikon CiL upright microscope with a color camera using Nikon Plan 4×/0.1, 10×/0.25, 20×/0.4, 40×/0.65, and 100×/1.25 objectives. Structures in these tissues requiring annotation were done so according to this key: "GC"/granulosa cells, "TEC"/theca endocrine stroma, "TSC"/theca-derived stroma, and "CL"/corpus luteum.

Cell-type definitions.

Structures in the ovarian tissues requiring annotation include granulosa cells (GC), theca endocrine cells (TECs) that are derived from embryonic mesenchymal stromal cells in response to Hedgehog (HH) signaling [38], (TSC) theca-derived cells that eventually populate the stromal compartment, interstitial stromal cells that are derived from embryonic stromal fibroblasts [38], corpus luteum (CL), luteinizing follicle (LF), testicular Leydig cell (LC), testicular seminiferous epithelium (SE).

IFC cell counting and fluorescent level analysis.

Prepared images (2.3.3) of costained ovaries were subjected to cell-type counting as follows. First, SF1+ TEC cells were marked using the count analysis tool in Adobe Photoshop 2023. This was followed by counting NR2F2+SF1− stromal cells, then NR2F2− stroma, finally granulosa cells. Counts for each category were divided by the total number of cells counted in areas of a predefined size.

Because costains for NR2F2, SF1, and pMSK1 are nuclear and can be superimposed on nuclear Hoechst stain, their average levels can be measured simultaneously within and between cell types. For this analysis, cells were plotted according to their position in the ovary: theca, stroma, "GCs/A": granulosa cells in an antral follicle, or "GCs/PA" granulosa cells in a preantral follicle. The lasso tool in Adobe Photoshop was used to generate a mask around discrete regions of genetic material in the Hoechst channel. Subsequent layers representing NR2F2, SF1, and pMSK1 staining were then sampled in the histogram tool, which returns average intensity and standard deviation values for each channel. Composite graphs in Figure 5A–C include at least 200 independent measurements for each category listed above, representing the average intensity of NR2F2, SF1, or pMSK1 in each condition.

For stains exhibiting cytoplasmic staining, more relaxed sampling masks were generated over cells and also included the nucleus. In this case, additional parameters were imposed to sample the following regions: "Theca/A": or a theca region surrounding an antral follicle, "Stroma": from a mixed-cell type interstitial nest, and "GC/A": granulosa cells in an antral follicle. Because masks segmenting the cellular regions are imprecise, it better serves as an estimation of relative levels of protein content in a region. While most of the changes documented in Figure 5A–C are concordant with Figure 5D and E, variation was noted in the TSC (stromal compartment), which is likely due to the inherent complexity of the stromal compartment in the DHT-treated ovaries.

Statistical analysis

A Student *t*-test was used to evaluate statistical significance as follows: $*P < 0.05$, $**P < 0.01$, and $***P < 0.001$ in figures where statistical tests are employed. Statistical significance was measured relative to the WT condition unless otherwise specified.

Results

Morphology and gene expression profiles in WT and cKO ovaries

In ovaries of immature mice, the induction of VCAM1 in response to DHT occurred preferentially in SF1+ steroidogenic TECs and theca-derived stromal cells (TSCs) (Figure 1A) and coincided with stable nuclear localization of AR (Figure 1B). While stable nuclear AR in theca cells is often observed in WT cycling ovaries, nucleation of AR in stromal cells outside the theca layer is not [25]. Theca endocrine SF1+ cells also express NOTCH1, a receptor of the Notch signaling pathway, providing another specific functional marker of these cells in growing follicles (Figure 1C). By contrast, NOTCH2 is selectively expressed in granulosa cells of growing follicles and luteal cells of functional corpora lutea [39–43] (Supplementary Figure S1).

To determine the functional roles of VCAM1 and NR2F2 in theca cells and ovarian stromal cells, we utilized mice bearing floxed (*fl*) alleles for *Vcam1* or *Nr2f2* that were mated to *Cyp17a1*-iCRE mice (cKOs) thus targeting deletion of each gene selectively to androgen-producing cells in female and male mice (Figure 1D). Ovarian sections from age-matched control (AMC) WT, *Vcam1*, and *Nr2f2* cKO mice were stained with H&E and ovarian markers CYP11A1/SF1 to determine the ovarian morphologic phenotypes in the mutant mice (Figure 1E and F). Ovaries in WT mice exhibited numerous corpora lutea (CL), follicles at different stages of preantral to antral development, and dense stromal tissue (TSC). By contrast, the *Vcam1* and *Nr2f2* cKO ovaries displayed altered stromal, follicular, and luteal tissues. Immunofluorescence (IF) images revealed impaired expansion of the SF1+/CYP11A1+ theca stromal cells and poor follicle integrity (especially small follicles) in *Nr2f2* cKO mice compared to AMC (Figure 1F). *Vcam1* cKO ovaries contained more SF1+ TSCs and CL that expressed CYP11A1 (Figure 1F). To assess endocrine profiles of the female mice, serum levels of LH, FSH, estrogen (E2), and progesterone (P4) were measured (Figure 1G). Despite normal levels of FSH and LH and the presence of CYP11A1+ CLs (Figure 1E and F) in the mutant mice, serum levels of progesterone were low in the *Vcam1* and *Nr2f2* cKO mice (Figure 1G).

Transcript analyses

Quantitative PCR analyses documented successful depletion of *Vcam1* and *Nr2f2* transcript levels in whole ovarian mRNA in both cKO mouse lines (Figure 2A). Ovarian transcripts were also analyzed to assess the expression of steroidogenic genes, signaling hormones, indicators of luteal function, and markers for granulosa cells (Figure 2B and C). Selection of these genes was based on a pilot RNAseq experiment independently reestablished in new pooled sets of RNA. The *Vcam1* cKO female ovary exhibited increases in the transcript levels for *Nr2f2* mRNA, while the levels of *Fshr*, *Runx2*, and *Akr1c18* (20αHSD) that metabolizes progesterone to an inactive progestin were decreased. Transcript expression of theca and luteal cell enriched genes *Cyp11a1* and *Insl3* was low in *Nr2f2* cKO mice whereas *Akr1c18* increased compared to controls (Figure 2B). Levels of *Amh* were also increased in the *Nr2f2* cKO mice.

Immunolocalization of proteins

To assess the specific expression and localization of proteins in theca cells, IF imaging was utilized on sections of AMC and cKO mutant mouse ovaries (Figure 2D–F). NOTCH1 was present in TECs, granulosa cells, and in SF1− stromal cells in the WT AMC and cKO ovaries. Immunofluorescence imaging additionally revealed complex NOTCH1 localization in a cell type-specific manner: (1) some SF1+ granulosa, TECs, and TSCs exhibit nuclear NOTCH1 localization; (2) strips of SF1−/NOTCH1+ (cytoplasmic/nuclear) populations line the theca interna; (3) and a population of NOTCH1+ cells invade luteal structures and are likely vascular related.

Based on the low levels of serum progesterone in the cKO females (Figure 1G), and specific changes in transcripts (Figure 2), we immunolocalized INSL3 and 20αHSD (*Akr1c18*) with SF1 in WT and cKO ovaries. INSL3 was present in CL, theca, and stromal cells in the WT AMC ovary (Supplementary Figure S2A). The *Vcam1* cKO ovary

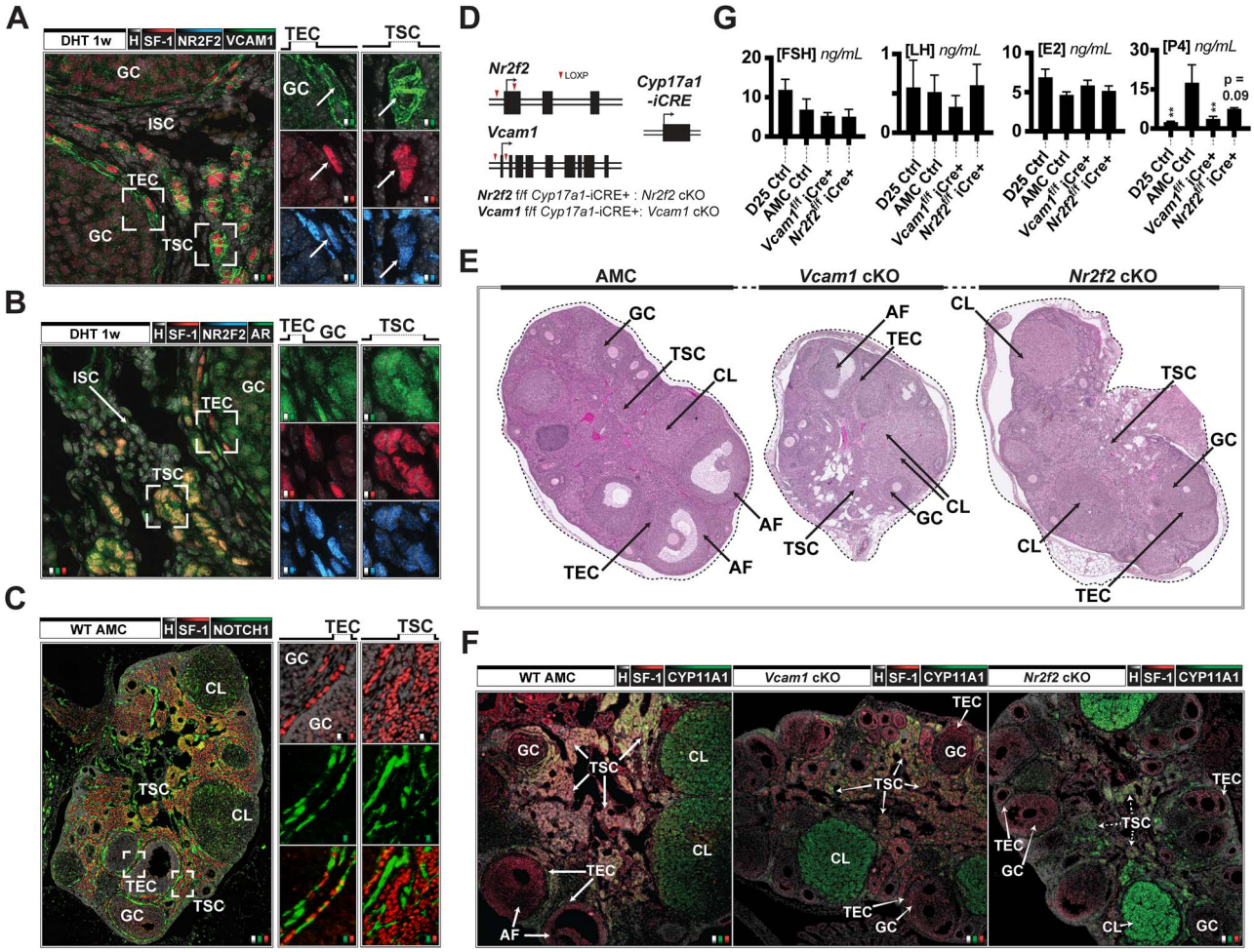

Figure 1. Strategy to determine the impact of targeted VCAM1 or NR2F2 loss on androgen-producing cells in ovarian function. (**A**) Representative DHT-treated ovary, IF costained for SF-1, NR2F2, and VCAM1. (**B**) Matched costain to (A), alternatively for AR. (**C**) Costain for SF1 and NOTCH1 in a WT pubertal female ovary. (**D**) VCAM1 (*Vcam1* f/f) and NR2F2 (*Nr2f2* f/f) mice mated into *Cyp17a1*-iCRE mice, yielding *Vcam1* or *Nr2f2* cKO females and males. (**E**) Representative H&E stains for control and cKO ovaries. (**F**) IF costaining of 2-month-old WT (AMC), *Vcam1* cKO, and *Nr2f2* cKO ovaries costained for SF-1 and CYP11A1. (**G**) Serum FSH, LH, estradiol (E2), and progesterone (P4) measurements in females ($N = 4$). Abbreviation key in materials and methods.

contained a reduced number of corpora lutea, which expressed lower levels of INSL3. However, the *Vcam1 cKO* ovary retained INSL3 expression in theca and antral follicles when compared to the WT ovary (Supplementary Figure S2B). Consistent with the decreased *Insl3* mRNA in *Nr2f2* cKO ovary, INSL3 immunostaining was reduced in the *Nr2f2* cKO female ovary relative to the WT or *Vcam1* cKO condition (Supplementary Figure S2C).

By contrast, expression of 20αHSD (*Akr1c18*) was selectively expressed in corpora lutea undergoing regression in the WT AMC ovary (Supplementary Figure S2D). Levels of 20αHSD (and transcript) were persistently low in the *Vcam1* cKO female ovaries (Figure 2B, Supplementary Figure S2E), whereas higher relative levels of *Akr1c18* transcript and 20αHSD protein were observed in *Nr2f2* cKO ovaries (Supplementary Figure S2F). These results suggest that altered expression of INSL3 and 20αHSD likely contributed to the reduced levels of serum progesterone in the cKO female ovaries (Figure 1G), but that the mechanisms impacting progesterone levels in the cKO females likely differ.

PCOS phenotype: impact of DHT on tissue morphology and cell-specific expression of regulatory proteins in control and mutant mouse ovaries

To determine the impact of androgens on ovarian morphology and theca cell functions, we analyzed the expression and localization of specific theca-associated proteins, CYP11A1, αSMA, VCAM1, NOTCH1, and pMSK1, in ovaries of control and mutant mice treated with DHT. Expression of CYP11A1, like that of VCAM1, co-localized in SF1+ TEC in WT + DHT control mice (Figure 3A). CYP11A1 was also expressed in mural layer of granulosa cells and cumulus–oocyte complexes (COCs) of several growing follicles in these mice. While the level of CYP11A1 protein was unchanged in the TECs/TSCs of *Vcam1* cKO + DHT ovary, it was visibly reduced in antral follicles (Figure 3B). Drastic alterations in the ovarian stromal compartment were noted in the *Nr2f2 cKO* + DHT ovaries: SF1+ TEC cells were rare around antral follicles and very few TSCs were present in the ovarian stroma. However, SF1 and CYP11A1 were expressed in granulosa cells of antral

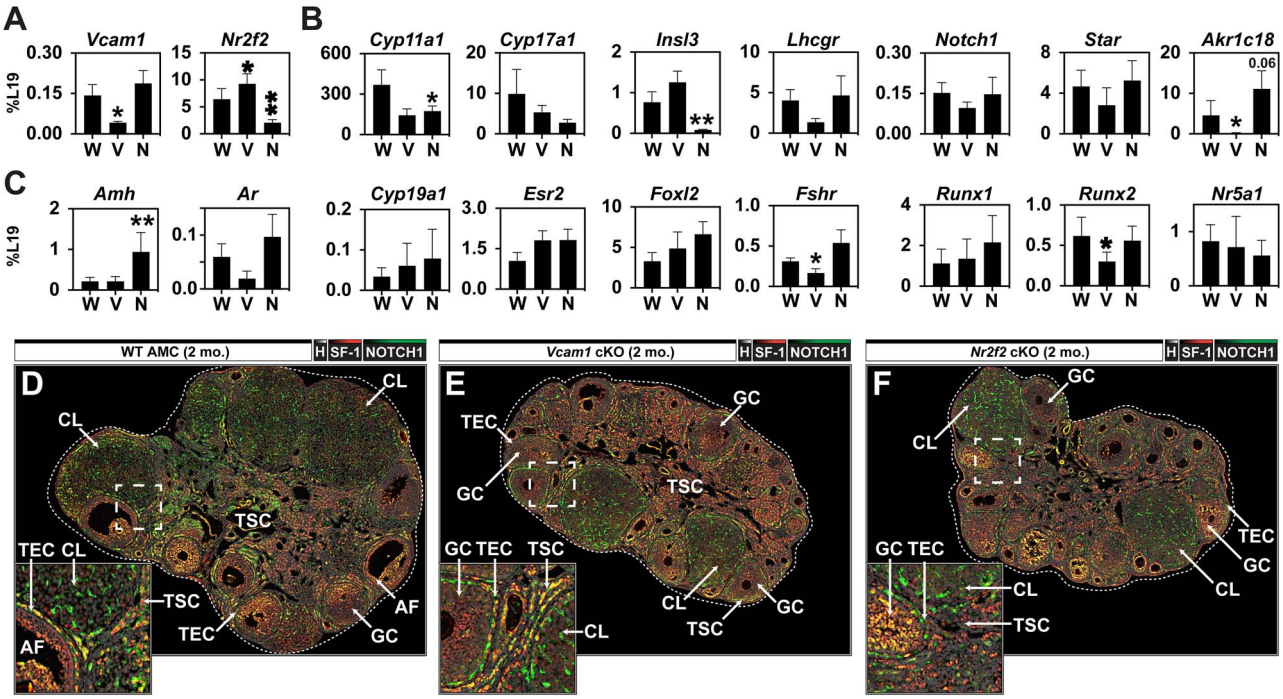

Figure 2. Transcript analysis of steroidogenic regulatory genes of theca, granulosa, and luteal cells with tissue validation. (**A**) Measurement of *Vcam1* and *Nr2f2* mRNA in isolated whole ovary from WT, *Vcam1* cKO, and *Nr2f2* cKO animals ($N = 7$). (**B**) Transcript levels for ovarian theca- and steroidogenesis-associated markers were observed ($N = 4+$). (**C**) Transcript levels for granulosa- and luteal-associated genes in WT and cKO ovaries. (**D**) WT control ovary costained for SF-1 and NOTCH1. (C) Age- and stain-matched *Vcam1* cKO ovary. (D) *Nr2f2* cKO ovary. "W": wild-type, "V": *Vcam1* cKO, "N": *Nr2f2* cKO (pubertal cycling).

follicles similar to that observed in ovaries of WT + DHT mice (Figure 3C).

In WT DHT-treated mice, VCAM1 was expressed in SF1+ TECs and in the granulosa/cumulus of growing follicles (Figure 3D). In the DHT-treated *Vcam1* cKO ovaries, VCAM1 expression was disrupted in SF1+ theca cells (relative to WT), but was detected in some granulosa and cumulus cells (Figure 3E). Because the stromal compartment was depleted in the *Nr2f2 cKO* ovaries, DHT-induced VCAM1 expression in SF1+ TECs was also reduced (Figure 3F). The detection of VCAM1 protein in granulosa cells contrasted with previous observations [25] which reported that androgen-dependent VCAM1 induction was restricted solely to theca in the ovary. Two differences may explain the outcomes: (1) a shorter exposure time to the DHT treatment, which was done to lessen the metabolic impacts of prolonged DHT treatment used in the previous study; and (2) the extracellular domain of VCAM1 can be cleaved and released as a soluble factor independent from the cell producing VCAM1 [44].

DHT has been shown to induce the expression of LH receptor (LHCGR) transcripts in granulosa cells of growing follicles in immature mice [45]. Therefore, we additionally analyzed the impact of DHT on the expression LHCGR using mice expressing HA-tagged LHCGR in vivo [37]. In the DHT-treated WT mice, HA-tagged LHCGR was detected in the ovary in the locations depicted: SF1+ TEC/TSC cells, discreet granulosa cells associated with later stage follicles, and in the ovarian surface epithelium, where it was double positive with SF1 (Supplementary Figure S3A). Also striking was the expression of HA-LHCGR in SF1+ granulosa cells present in a small growing follicle. This was not observed in normal growing follicles of a similar size. In normal wild-type mice, LHCGR is only induced in granulosa cells of preovulatory follicles where it is essential for LH induction of ovulation, cumulus–oocyte expansion, and luteinization [46]. Costains for NR2F2 alone (w/Hoechst) documented the depletion of NR2F2 protein in both cKO ovaries + DHT relative to the WT + DHT controls (Supplementary Figure S3B).

Additional stains were done to colocalize NOTCH1 with SF1/αSMA in the WT and *Nr2f2* cKO ovaries. This served to better delineate myofibroblast and steroidogenic lineages in the ovarian stromal compartment, and to assess the impact of DHT on NOTCH1 staining in each compartment. In the WT DHT-treated ovaries, SF1+ TEC/TSC cells were distinctly separate from αSMA+ cell types (Figure 4A). In this scenario, NOTCH1 is highly expressed in TECs but not in αSMA+/SF1− stromal cells of WT DHT-treated ovaries (Figure 4B). Furthermore, robust and consistent nuclear NOTCH1 co-localized with SF1 in TECs, TSCs, and GCs (Figure 4C). This response to androgens was modified in the *Nr2f2* cKO background characterized by poor maintenance of the steroidogenic SF1+ lineage in theca of large follicles, a reduction in the levels of αSMA lining the theca of large follicles, reduced expansion of TSCs into the ovarian stromal compartment, and higher relative levels of SF1 in granulosa cells (Figure 4D). While NOTCH1+ cells lining follicles are present in the theca of the DHT-treated *Nr2f2* cKO ovary, NOTCH1 staining was reduced in the *Nr2f2* cKO ovary + DHT especially in SF1+ TEC/TSCs (Figure 4E and F). By contrast, high levels of NOTCH1 costained with SF1 in granulosa cells of the *Nr2f2* cKO mice (Figure 4F).

Quantitative analysis of the factor distribution in the ovary

In previous studies, we identified pMSK1 (phospho-Thr581-mitogen- and stress-associated kinase) as a proliferation marker in human carcinoma xenograft tissues in mice [47].

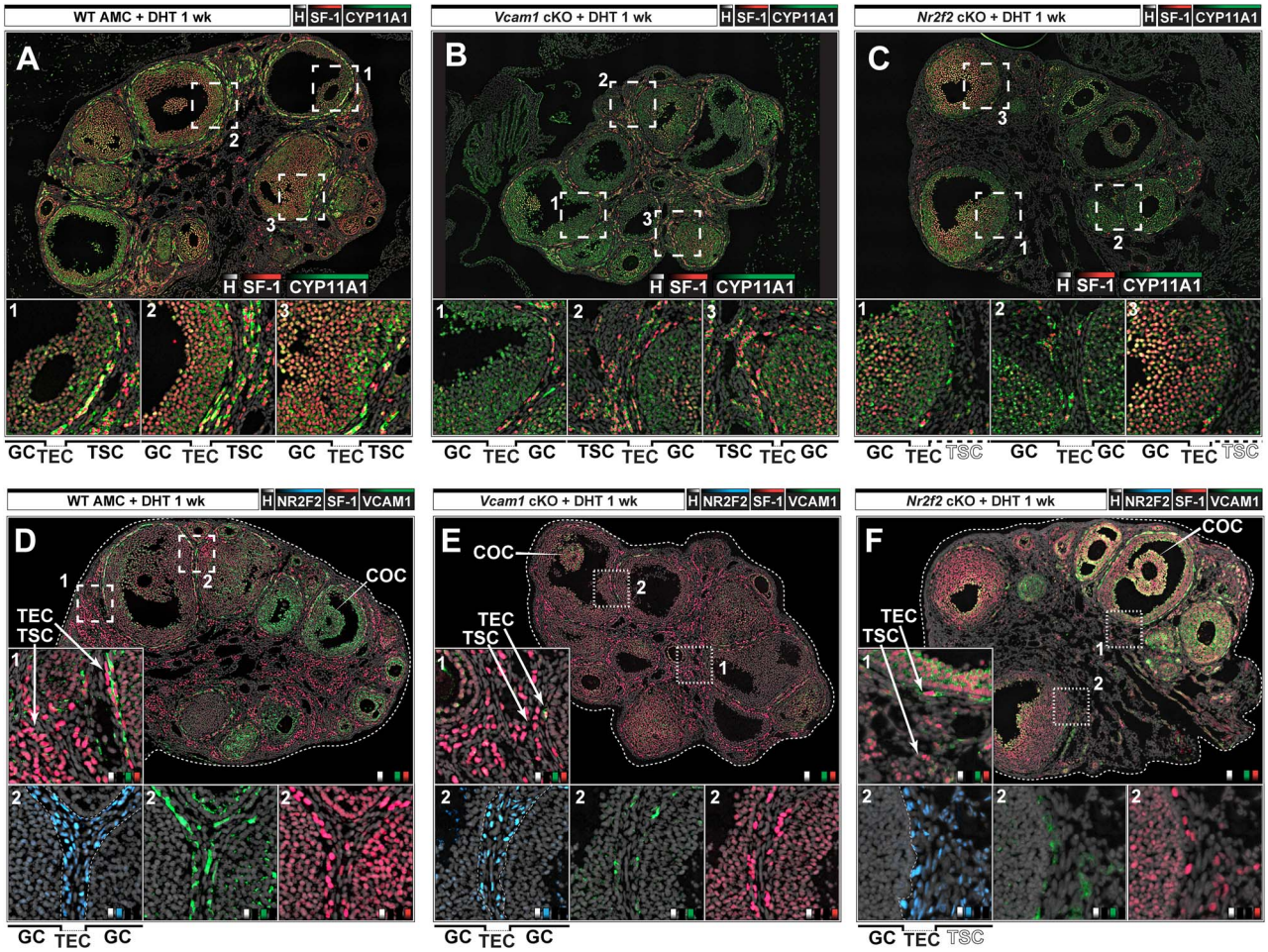

Figure 3. Targeting VCAM1 deletion to SF-1+ theca cells: altered responses to androgens and impacted steroidogenesis. (**A**) Representative WT DHT-treated ovary IF costained for Hoechst, NR2F2, SF-1, and CYP11A1. Zoomed costains in insets are identified by column "1", "2", or "3". (**B**) Matched androgenized *Vcam1* cKO ovary similarly depicted. (**C**) *Nr2f2* cKO ovary. (**D**) Representative WT DHT-treated ovary IF costained for NR2F2, SF-1, and VCAM1. (**E**) Matched androgenized *Vcam1* cKO ovary similarly depicted. VCAM1 was efficiently deleted in SF-1+ TEC cells. (**F**) The androgenized *Nr2f2* cKO ovary becomes devoid of SF-1+ TSC populations.

Here, we show that pMSK1 (Thr581) brightly marked mitotic granulosa and theca cells in non-cancerous ovarian tissue (Figure 4G–I). To evaluate potential changes in the composition of the ovary following targeted gene deletion of *Vcam1* or *Nr2f2* (all +DHT), cells were grouped into categories and counted. This is detailed in the Materials and Methods. The number of SF1+ TEC/TSCs in the *Nr2f2* cKO females is decreased relative to WT, but is unchanged in the *Vcam1* cKO mice (Figure 5A). This contrasted with the NR2F2+SF1− population counts, which were similarly reduced in both the *Vcam1* and *Nr2f2* cKO mice. More NR2F2/SF1 −/− cells were observed in the *Nr2f2* cKO females, but not in the *Vcam1* cKO females. Finally, more total granulosa cells were counted in the *Vcam1* cKO females, but not in the *Nr2f2* cKO females. Thus, targeted gene deletion revealed overlapping (category 2) and distinct (category 1, 3, 4) changes in the composition of the WT and cKO ovaries.

All the IF markers in Figure 4G–I are nuclear markers, making them amenable to individual measuring segmented by chromatin (Hoechst) in all three layers simultaneously (Figure 5B). Cells were first counted according to their *position in the ovary* relative to follicles, represented as theca, stroma, GCs ("PA", preantral), or antral GCs ("A"). An example set of five cells shown in Figure 5B was used to determine the intensity values for NR2F2, SF1, and pMSK1 in each measured cell. At least 200 cells were analyzed in each category and image set in Figure 4G–I, revealing changes in the levels for these markers in a compartment-specific manner.

First, NR2F2 levels drop precipitously in the *Vcam1* and *Nr2f2* cKO females in both theca and stroma (Figure 5C, Supplementary Figure S3B). SF1 levels in the theca of both cKO lines were unchanged in this analysis, but were significantly reduced in the *Nr2f2* cKO stroma (Figure 5C). Dramatic induction of SF1 in the granulosa cells (both PA and A) following DHT was observed only in the *Nr2f2* cKO females. In agreement with the staining, pMSK1 levels were detected at lower levels in both *Vcam1* and *Nr2f2* cKO females in theca and stroma (Figure 5C). Decreased pMSK1 was also observed in the granulosa cells of *Vcam1* cKO but not in the *Nr2f2 cKO* ovaries. Collectively, measuring the levels of the factors simultaneously served as a powerful tool to quantify the levels of these factors in ovaries of each genotype.

To measure the levels of factors localizing to the cytoplasm, more relaxed masks were generated (as in Figure 5B) to sample a continuous region of interest composed of smaller subregions (200 in each category) individually representing a

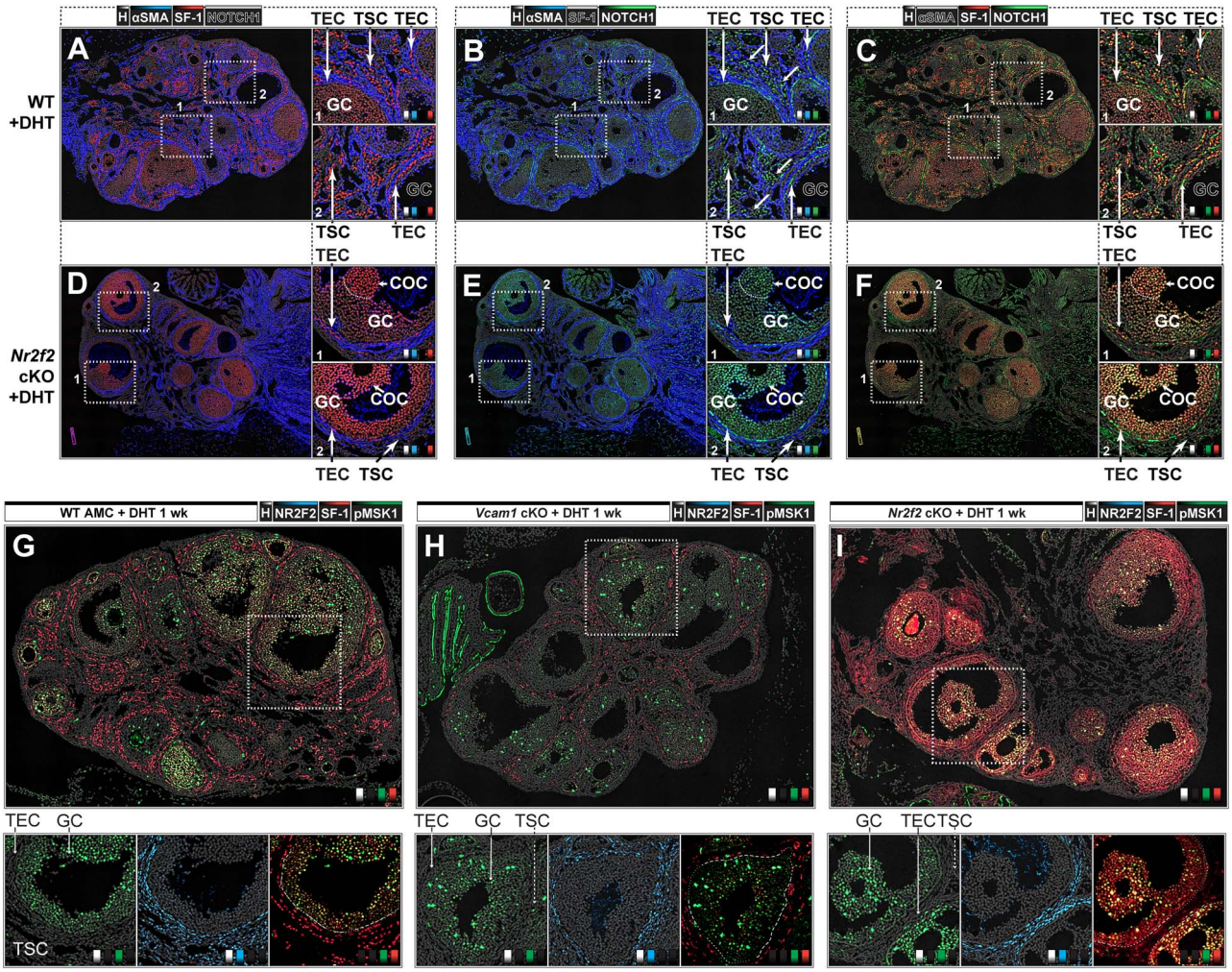

Figure 4. Assessing proliferation and NOTCH1 localization in the DHT-treated WT and cKO ovaries. (**A**) WT + DHT ovary costained for αSMA, SF1, and Hoechst. (**B**) Previous section in (A) with αSMA and NOTCH1 visible. (**C**) Section in (A) with SF1 and NOTCH1 visible. (**D**) Nr2f2 cKO ovary stained for αSMA, SF1, and Hoechst. (**E**) Previous section in (D) with αSMA and NOTCH1 visible. (**F**) Section in (D) with SF1 and NOTCH1 visible. (**G**) WT androgenized ovary IF costained for Hoechst, NR2F2, SF-1, and pMSK1 (Thr581). MSK1 is highly phosphorylated in dividing cells in tissue. (**H**) Representative *Vcam1* cKO ovary. (**I**) *Nr2f2* cKO ovary.

single cell and its cytoplasm (Figure 5D). Category definitions, additional parameters (relative to Figure 5B), and other considerations are detailed in the Materials and Methods. First, NR2F2 levels were depleted in "Theca/A" and "Stroma" categories of both *Vcam1* and *Nr2f2* cKO mice + DHT relative to WT + DHT (Figure 5E). While SF1 levels were reduced in both the "Theca/A" and "Stroma" tissues of the *Nr2f2* cKO mice + DHT, the *Vcam1* cKO + DHT ovary exhibited reduced SF1 content only in the "Stroma" category. Conversely, SF1 content increased substantially in antral granulosa cells of the *Nr2f2* cKO females. Changes in the levels of CYP11A1 in these regions mirrored the changes observed in the SF1 content in "Theca" and "Stroma" tissues of WT and cKO female ovaries + DHT. Expression of CYP11A1 was decreased only in the *Vcam1* cKO female antral granulosa cells. Levels of αSMA were significantly reduced in both "Theca/A" and "Stroma" tissues of the *Nr2f2* cKO females + DHT relative to WT + DHT. Lastly, overall levels of NOTCH1 remained unchanged in the "Theca/A" category, were reduced in the "Stroma" category, and increased in the "GC/A" tissues of the *Nr2f2* cKO female + DHT ovary compared to WT.

PCOS phenotype: responses of mutant ovaries to gonadotropins

To assess the impact of gonadotropins in the cKO backgrounds, we treated immature (D25) WT and cKO females with 5 IU eCG (48 h) alone, or superovulated (5 IU eCG/48 h) followed by 5 IU hCG/24 h to stimulate antral follicular growth, ovulation, and early corpus luteum formation. Ovaries from eCG-treated WT mice (Figure 6A; H&E) showed antral follicles and early stages of corpus luteum formation. The *Vcam1* cKO + eCG ovary exhibited many healthy antral/preovulatory follicles, but no corpora lutea (Figure 6B; H&E). Ovaries of the *Nr2f2* cKO mice treated with eCG contained a few antral follicles and exhibited numerous corpora lutea and luteinizing follicles (Figure 6C; H&E).

To assess the functional characteristics of the WT and mutant ovaries, theca and luteal cell markers (CYP11A1, CYP17A1, SF1, and NR2F2) were analyzed in the eCG-treated mice. CYP11A1 protein was highly expressed in TEC/TSC and luteinized cells of eCG-treated WT mice (Figure 6A) but was not observed in the *Vcam1* cKO + eCG

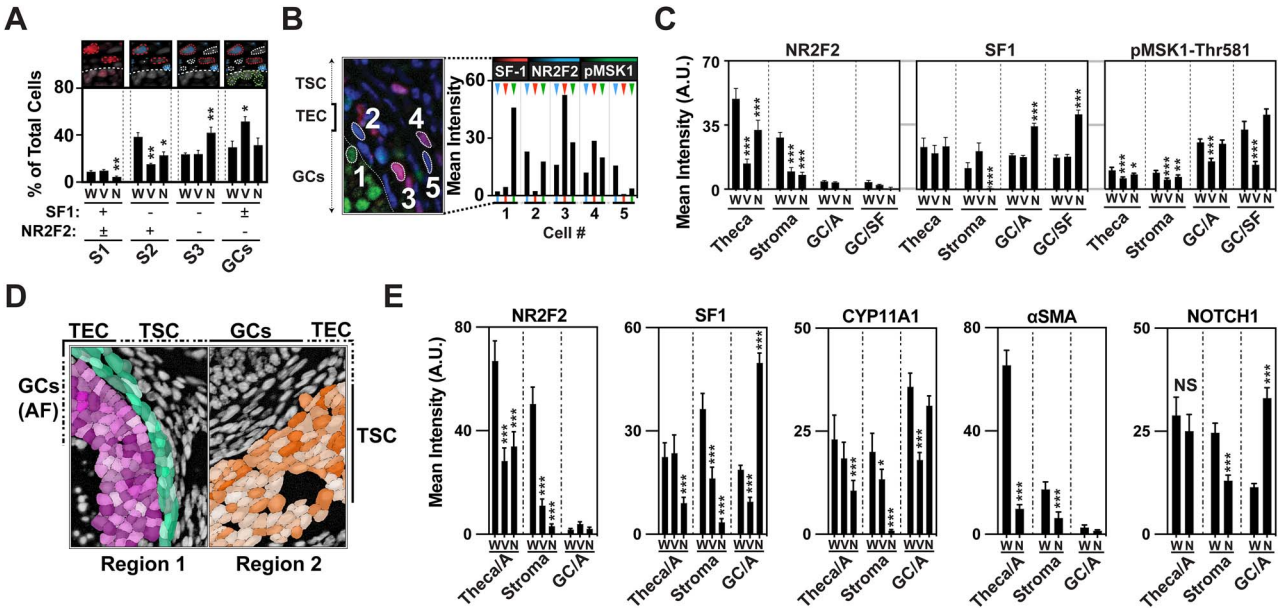

Figure 5. Quantification of NR2F2, SF1, pMSK1, αSMA, and NOTCH1 levels in DHT-treated WT and cKO ovaries. (**A**) Proportion of cells counted in (**A**)–(**C**) representing SF1+, NR2F2+SF1−, NR2F2−SF1−, or granulosa cell populations following DHT treatment in the WT and cKO female ovary. (**B**) Strategy to measure the relative fluorescent intensity of NR2F2, SF1, and pMSK1 in individual cells based on their location in the ovary: theca (cell 2, 3), stroma (cell 4, 5), preantral granulosa cells (cell 1), or antral granulosa cells. Average intensity values for cells 1–5 are plotted to the right of the example immunolabeled image. (C) Levels of fluorescence of NR2F2 for 200+ cells averaged in each condition (WT + DHT or cKO + DHT) and compartment detailed in 6D. This is followed by SF1 levels, then by pMSK1 levels. (**D**) Layer masks for markers requiring sampling in the cell cytoplasm were more permissive to encompass the estimated borders between cells in a continuous region defined by its location or function. In this case, 200 independent continuous regions in the theca/granulosa (both restricted to antral follicles "Theca/A" and "GCs/A") and steroidogenic TSC clusters were sampled. (**E**) Results of analysis detailed in (D), measuring the average levels of NR2F2, SF1, CYP11A1, αSMA, and NOTCH1. "W": wild-type, "V": *Vcam1* cKO, "N": *Nr2f2* cKO (All + DHT).

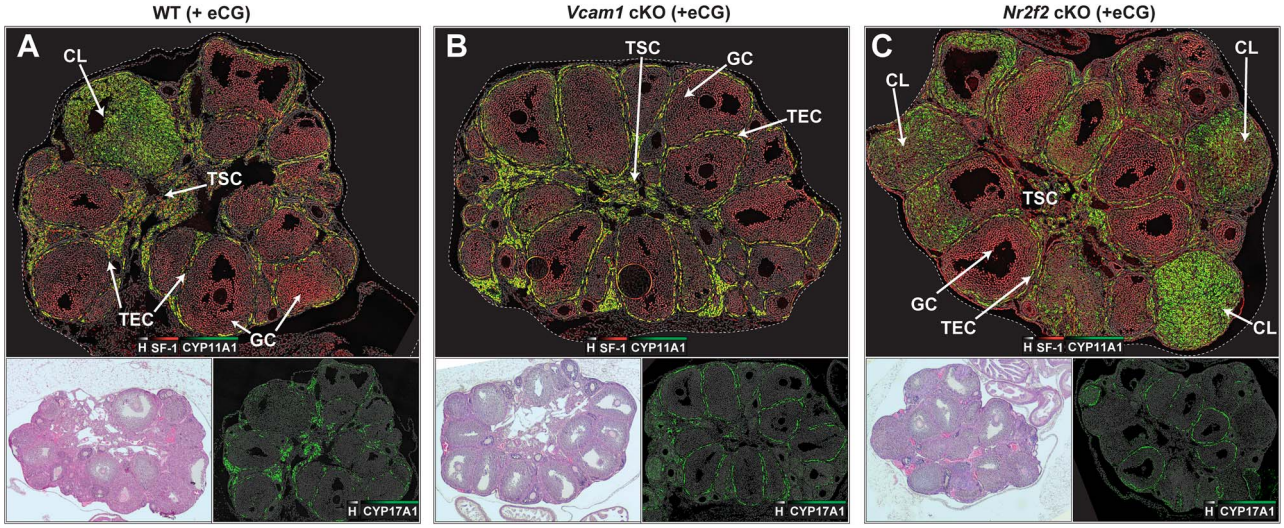

Figure 6. Assessing steroidogenesis in eCG-synchronized WT and cKO ovaries. (**A**) WT control ovary treated with eCG (48 h, 5 IU) costained with Hoechst, SF1, and CYP11A1 (top), representative H&E (insert, bottom left) or CYP17A1 (Hoechst: bottom right). (**B**) Representative eCG-treated *Vcam1* cKO ovary similarly depicted to (A). (**C**) *Nr2f2* cKO ovary treated with eCG.

mouse ovary that lacked corpora lutea (Figure 6B). *The Nr2f2* cKO mice lacked expansion of CYP11A1+ TSCs but contained an abnormally high number of CYP11A1+ corpora lutea-like structures, some quite small in size. These observations provide supporting evidence that NR2F2 depletion facilitates increased eCG-induced ovulation and luteinization (Figure 6C).

To assess androgen biosynthesis, staining for CYP17A1 was carried out on the eCG-treated WT and cKO ovaries. Staining for CYP17A1 in the WT + eCG ovary was high in TECs and TSCs (Figure 6A; inserts). In the *Vcam1* cKO ovaries, CYP17A1+ TECs were particularly abundant in the TEC (Figure 6B; inserts). While the *Nr2f2* cKO + eCG ovary recruited CYP17A1+ TECs to follicles, this response was attenuated around numerous luteinized structures, which were also CYP11A1+ (Figure 6C; inserts).

Although tonic LH drives ovarian theca cell androgen biosynthesis, the LH surge dramatically suppresses this

steroidogenic function. To evaluate the recruitment of androgen-producing cells in WT and cKO + eCG/hCG ovaries, similar IF costains were carried out on WT and cKO + eCG/hCG mice (Supplementary Figure S4). In ovaries of WT mice, CYP11A1 was high in TSC cells, luteal cells, and in TECs around small follicles (Supplementary Figure S4A). Ovaries of *Vcam1* and *Nr2f2* + eCG/hCG cKO mice contained numerous, normal appearing CYP11A1+ luteal structures. However, the number of TSCs was reduced in the *Nr2f2* cKO + eCG/hCG mice relative to WT and *Vcam1* cKO + eCG/hCG mice (Supplementary Figure S4B and C). Consistent with morphological images and expression of theca and luteal cell markers CYP11A1, CYP17A1, SF1, and NR2F2 (Supplementary Figure S4), the eCG/hCG-treated *Nr2f2* cKO females ovulated significantly more oocytes (52.4 ± 8.0; $*P < 0.05$) than the WT (33.5 ± 4.4; oocytes) or *Vcam1* cKO mice (32.6 ± 10.3; oocytes). Ovulated oocytes were isolated and counted from the oviduct following 48 h of eCG/24 h of hCG. Previous studies also documented that immature mice exposed to DHT ovulated in response to eCG/hCG treatment, but the number ovulated was lower in the DHT-treated +eCG/hCG mice compared to non-treated eCG/hCG controls (NT: 25 ± 5; DHT-treated 12 ± 5) [25]. Furthermore, eCG/hCG-treated cKO mice exhibited no visible difference in the suppression of CYP17A1 expression following ovulation and luteinization.

The expression/localization of NOTCH1 and INSL3 were also modified following eCG treatment. First, WT + eCG ovaries exhibited (1) NOTCH1 staining in SF1+ TECs, TSCs, and GCs; (2) an SF1− population of theca cells with NOTCH1 expressed in the TEC and TSC compartments; and (3) a population of SF1−/NOTCH1+ cells that invade luteal structures (Figure 7A). The *Vcam1* cKO + eCG mice exhibited higher levels of NOTCH1+ cells in the TSC compartment relative to WT + eCG mice, as well as populations of SF1+ TEC/TSC exhibiting both cytoplasmic and nuclear NOTCH1 localization (Figure 7B). This pattern contrasted with that observed in ovaries of the *Nr2f2* cKO + eCG females where NOTCH1 was visibly reduced in the TECs/TSCs, and that the SF1−/NOTCH1+ cells invading luteal structures were more frequent than in the WT or *Vcam1* cKO + eCG mice (Figure 7C).

The level of *Insl3* transcripts in the adult *Nr2f2 cKO* ovaries was lower than WT or *Vcam1* cKO non-treated pubertal females (Figure 2B). To determine the relative abundance of INSL3 protein in WT and cKO ovaries, immunodetection of INSL3 and SF1 were carried out specifically in the eCG-treated mice. WT + eCG ovaries exhibited staining for INSL3 in the theca of select follicles, certain TSCs, and in CL (Figure 7D). The *Vcam1* cKO + eCG mice displayed lower relative amounts of INSL3 staining in the TEC compartment, retained INSL3 in SF1+ TSCs in the stroma, but lacked CLs for comparison to those observed in the WT + eCG female (Figure 7E). The *Nr2f2* cKO exhibited significantly lower staining of INSL3, mainly in TSC and CL tissues relative to WT + eCG (Figure 7F). This is in agreement with the transcript and staining data (Figure 2) and INSL3 levels were low in luteinized structures that expressed high levels of CYP11A1 (Figure 6B).

In WT + eCG/hCG females, NOTCH1 was expressed in SF1+ TECs/TSCs and in non-steroidogenic (SF1−) cells in the theca and stroma, while NOTCH1+/SF1− cells invade certain populations of CL (Supplementary Figure S5A). The *Vcam1* cKO + eCG/hCG females continued to generate a population of cells exhibiting cytoplasmic and nuclear staining for NOTCH1 in TECs/TSCs (Supplementary Figure S5B). The impacts of *Nr2f2* cKO on responses to eCG/hCG resulted in reduced number of SF1+ TECs/TSCs also exhibiting lower amounts of NOTCH1 relative to WT + eCG/hCG (Supplementary Figure S5C). Invasion of CL by SF1−/NOTCH1+ cells was more prominent in the *Nr2f2* cKO + eCG/hCG females relative to WT + eCG/hCG females.

Expression of INSL3 was altered by eCG/hCG in the WT and cKO mice. In WT mice + eCG/hCG, INSL3 expression was lower in TECs, continued to be expressed in TSCs, and in certain populations of CLs (Supplementary Figure S5D). The response of *Vcam1* cKO + eCG/hCG was indistinguishable from WT + eCG/hCG mice. The *Nr2f2* cKO + eCG/hCG females additionally generated a population of spindle-shaped SF1+ cells in the stromal compartment. These results also indicated that the expression of INSL3 in corpora lutea is variable and perhaps transient during the early stages of corpus luteum formation compared to adult control mice at 2 months of age (Figure 2). This indicated that other NR2F2-independent mechanisms likely regulate INSL3 expression in the luteal cells that do not express NR2F2. While the expression of NOTCH1 was selectively expressed in theca cells following eCG/hCG, NOTCH2 was highly expressed in granulosa cells of growing follicles as well as in corpora lutea following eCG and eCG/hCG treatments (Supplementary Figure S6).

Phenotypes of VCAM1 and NR2F2 KO male mice

VCAM1 and NR2F2 are also expressed in androgen-producing Leydig cells within the testis [48] and have been depleted in the *Nr2f2* cKO and *Vcam1* cKO mouse lines generated in these studies (Figure 8A). To determine the impact of the Leydig cell-specific KO on these genes, we analyzed testis samples from D25 (prepubertal control), AMC, *Vcam1* cKO, and *Nr2f2* cKO mice. First, fixed embedded tissue was stained for SF1 to determine the number of SF1+ Leydig cells in each condition. *Vcam1* cKO testes contained more SF1+ Leydig cells relative to age-matched controls, while fewer SF1+ Leydig cells were observed in the *Nr2f2* cKO males (Figure 8B). Transcript analysis on revalidated targets identified in RNAseq analysis identified *Insl3* as dramatically downregulated in the *Nr2f2* cKO males, but trended higher in *Vcam1* cKO males (Figure 8C), a pattern similar to the one observed in females (Figure 2A). Levels of *Cyp11a1* trended downward in the *Nr2f2* cKO males, while *Cyp17a1* levels trend higher in *Vcam1* cKO males (Figure 8D). Consistent downregulation of *Apoc1*, or apolipoprotein C1, was observed in the *Nr2f2* cKO males, which trended higher in the *Vcam1* cKO males. Levels of *Tpsb2*, a mast cell marker, were dramatically higher in the NR2F2 cKO males. Collectively, these changes indicate impairments in multiple compartments critical for steroidogenesis following cKO in the testis.

To probe the tissue localization of these factors, prepubertal (D25) and adult (2 month) testis samples were fixed and stained for NR2F2, SF1, CYP11A1, CYP17A1, and INSL3. First, CYP11A1 was present at low levels in immature SF1+ Leydig cells (Figure 8E). By 2 months, CYP11A1 levels increased and additionally occupied long filaments (likely mitochondria) in SF1+ cells (Figure 8F). NR2F2 levels were

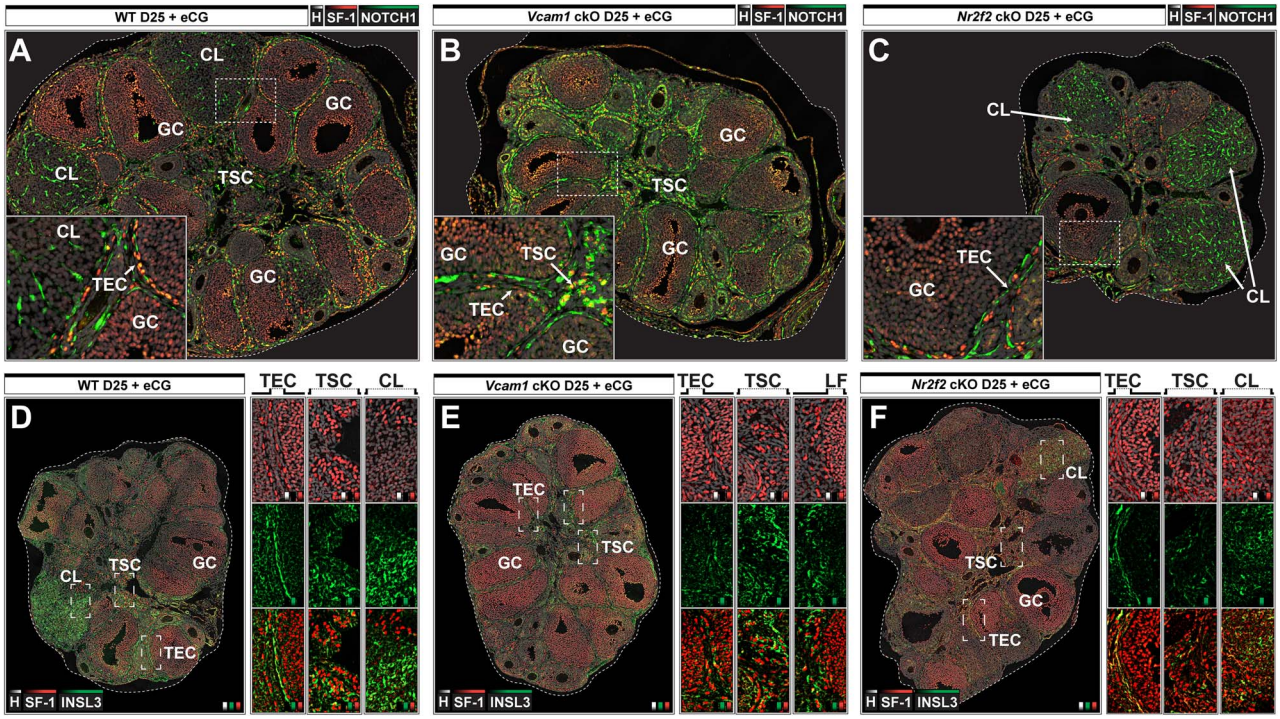

Figure 7. Assessing NOTCH1 and INSL3 levels in eCG-treated WT and cKO ovaries. (**A**) IF costain for Hoechst, SF1, and NOTCH1 in an eCG (48 h)-treated WT ovary. Zoomed inset depicted to the bottom left. (**B**) Similarly stained and imaged *Vcam1* cKO + eCG ovary relative to (A). (**C**) *Nr2f2* cKO ovary. (**D**) IF costain for Hoechst, SF1, and INSL3 in an eCG-treated WT ovary. Insets the TEC, TSC, and CL/LF regions are zoomed depicted separately. (**E**) *Vcam1* cKO + eCG ovary relative to (D). (**F**) Nr2f2 cKO + eCG ovary.

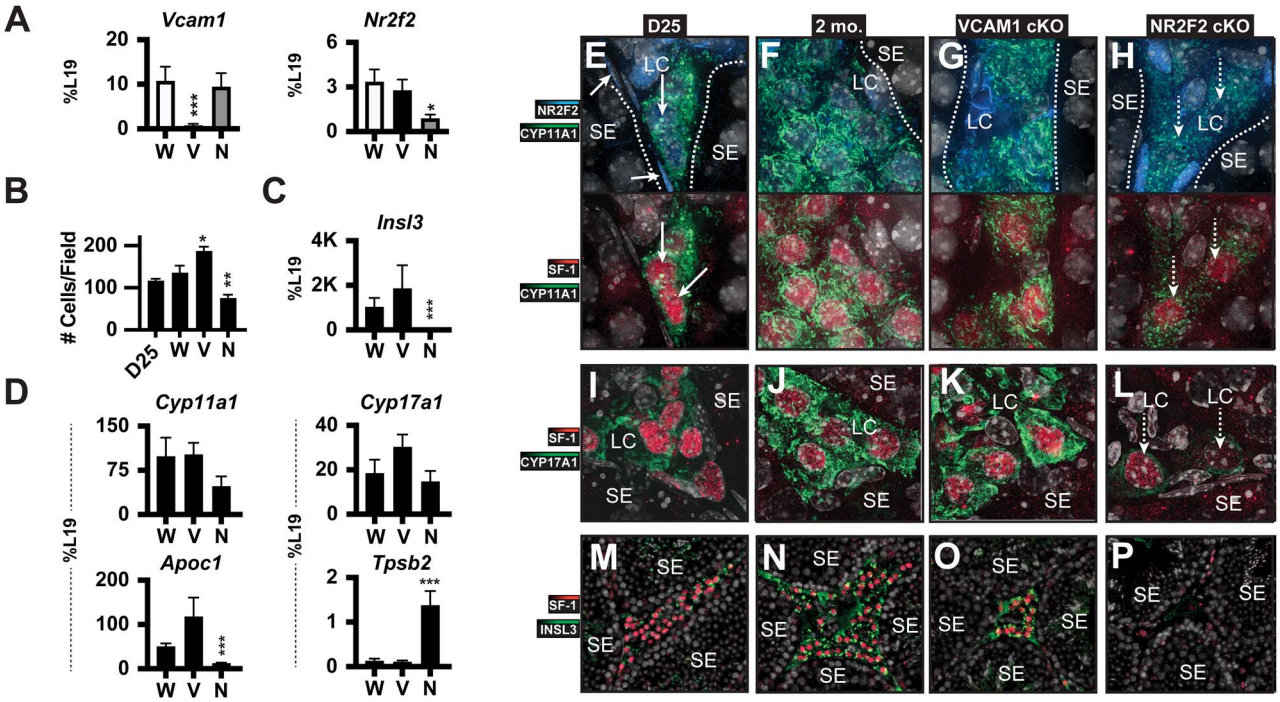

Figure 8. Assessing steroidogenesis in the cKO testis, commonalities, and differences with the ovary. (**A**) Levels of *Vcam1* and *Nr2f2* transcripts in the *Vcam1* cKO (V) and *Nr2f2* cKO (N) relative to WT control ("W"). (**B**) D25 (prepubertal), WT (2 mo.), *Vcam1* cKO, and *Nr2f2* cKO testis were stained for SF1. Leydig cells positive for SF1 were counted. (**C**) Transcript levels of *Insl3* were measured in WT and cKO males ($N = 3$). (**D**) *Cyp11a1*, *Cyp17a1*, *Apoc1*, and *Tpsb2* transcript levels were measured ($N = 3$). (**E**) Representative WT D25 control testis costained for NR2F2 (top), SF-1 (bottom), and CYP11A1. (**F**) Pubertal control testis relative to (D). (**G**) *Vcam1* cKO testis. (**H**) *Nr2f2* cKO testis. (**I**) D25 control WT testis costained for SF-1 and CYP17A1. (**J**) Pubertal WT control testis. (**K**) *Vcam1* cKO testis. (**L**) *Nr2f2* cKO testis. (**M**) Prepubertal control testis costained for SF-1 and INSL3. INSL3 is low in this condition. (**N**) INSL3 protein is upregulated following pubertal onset in a WT control male. (**O**) VCAM1 cKO male. (**P**) Reflecting transcript analysis in (C), INSL3 levels in the NR2F2 cKO males were substantially lower in Leydig cells.

also low in pubertal Leydig cells. While mitochondrial branching was retained in *Vcam1* cKO testis tissue (Figure 8G), deletion of NR2F2 in Leydig cells (marked with hatched arrows) disrupted this pattern, indicating dysfunction of mitochondrial structures that emerge after the initiation of male-specific steroidogenesis and spermatogenesis (Figure 8H). Costains showed lower relative levels of CYP17A1 in the SF1+ Leydig cells associated with the endoplasmic reticulum in prepubertal testis (Figure 8I). CYP17A1 was increased in WT pubertal controls and in *Vcam1* cKO males (no qualitative difference) at 2 months (Figure 8J and K), but was significantly reduced in the *Nr2f2* cKO testis (Figure 8L). Poor maintenance of the SF-1+ cell lineage downstream of NR2F2 deletion is a probable cause of low CYP11A1 and CYP17A1 protein levels. Lastly, costains for Leydig cell-derived INSL3, a biomarker for Leydig cell functionality in males, is low in the prepubertal testis (Figure 8M) but was robustly induced within Leydig cells at 2 months (Figure 8N). INSL3 is likely secreted in a constitutive pathway following synthesis [15, 17]. While INSL3 expression was retained in the *Vcam1* cKO testis, it became almost entirely absent in the *Nr2f2* cKO testis (Figure 7O and P). Curiously, these cKO male mice are fertile supporting studies of other showing that these genes are more critical for early testis development.

Discussion

Results of these studies reinforce the essential roles of theca cells in regulating follicular development, ovulation, and luteinization in response to androgens and gonadotropins; and how abnormal production of androgens by theca cells in PCOS patients might disrupt these events leading to follicle arrest [1, 3, 23, 36]. Androgens and the androgen receptor impact not only granulosa cells but also theca cells that contribute significantly to the underlying etiology of PCOS [25]. Specifically, the seminal studies of Sheng Wu et al. [27] documented for the first time that targeted disruption of AR in theca cells selectively blocked the ability of excess androgens to induce a PCOS phenotype in mice *in vivo* and in our studies was shown to be associated with reduced expression of VCAM1, an androgen target gene in theca cells [25]. The steroid receptor co-regulator NR2F2 impacts steroidogenesis in the ovary [25, 31] and is selectively expressed in theca cells; it is not expressed in granulosa cells of growing follicles [25]. However, factors that regulate theca cell functions *in vivo* to impact follicle arrest have not been clearly defined. By analyzing mutant mice in which either the *Nr2f2* or *Vcam1* gene was selectively depleted in theca cells, we provide novel evidence that disrupting the expression of each gene revealed their distinct roles in determining not only theca cell functions but also granulosa cell functions and responses of these cells to androgens and gonadotropins. Thus, altering theca cells functions, including androgen production, can profoundly alter follicular development, ovulation, and luteinization.

KO phenotypes

In these studies, we have documented that disruption of theca cell expression of either *Nr2f2* or V*cam1* in *Cyp17a1*+ theca endocrine cells altered expression of specific genes/proteins not only in theca cells but also in granulosa cells, indicating precise functional interactions between theca cells and granulosa cells (see Graphical Abstract). Specifically, the poor expansion of steroidogenic theca cells and stromal cells in the *Nr2f2 cKO* females indicated that NR2F2 is critical not only for establishing theca cells [38] but also for maintaining this androgenic cell lineage that also expresses SF1, StAR, CYP17A1, and INSL3 in the adult ovary [11, 31]. Although corpora lutea are present in the adult knockout mouse ovaries, the number is low compared to that observed in control adult mice (Figure 2). Furthermore, while the corpora lutea of cKO females expressed CYP11A1, serum concentrations of progesterone were low (Figure 1G), indicating that luteinization is incomplete/defective in both mutant mouse models. By comparison to the *Nr2f2* mutant mice, disruption of *Vcam1* in theca cells did not markedly alter antral follicular growth, the development of steroidogenic NR2F2+/SF1+/CYP17A1+ theca cells or stromal compartments, or the presence of CYP11A1+ corpora lutea. However, serum progesterone levels in these mice were also low indicating that luteal cell functions were altered/impaired. Compared to WT controls, the *Vcam1* cKO mice exhibited lower relative levels of *Fshr*, *Runx2*, and *Akr1c18* mRNA (Figure 2). The levels of 20αHSD protein (product of *Akr1c18*) were also lower (Supplementary Figure S2D and E). Thus, the loss of either *Nr2f2* or *Vcam1* in theca cells altered luteinization in adult mice. We next observed distinct abnormal responses of these mutant mice to exogenous androgen (DHT) and gonadotropin treatments, indicating that disrupting theca cell expression of these genes impacts specific events in folliculogenesis.

PCOS phenotype: impact of DHT

When immature *Nr2f2* cKO mice were exposed to exogenous DHT to mimic a PCOS-like phenotype, major changes were observed not only in theca cells but also remarkably in granulosa cells that do not express NR2F2, most dramatic of which was the increased expression of SF1 and NOTCH1 in granulosa cells of preantral (Figure 5C) and antral follicles (Figure 5E). We additionally observed higher levels of VCAM1 in the COCs of growing, non-ovulated, antral follicles in these mice (Figure 3F). In sharp contrast, DHT did not markedly increase the low levels of SF1+ granulosa cells in antral follicles of control wild-type mice. Thus, SF1 may not be a direct androgen target gene in granulosa cells of normal growing follicles. Rather, specific factors emanating from control theca cells may act to suppress SF1 expression in granulosa cells, thereby preventing premature expression of steroidogenic and other genes during early stages of follicular development.

Previous studies have shown that estradiol can increase SF1 in granulosa cells, whereas FSH/hCG tend to decrease expression [8]. The presence of SF1, CYP11A1, VCAM1, and NOTCH1 in granulosa cells of the abnormal follicles present in the DHT-treated *Nr2f2 cKO* mice indicated that these cells had acquired an unexpected phenotype expressing genes/proteins normally restricted to theca cells. Thus, the impact of DHT on granulosa cells in the *Nr2f2* cKO background is distinct and might be related to changes in the expression and co-regulation of NR4A1, AR, and NR5A2 in granulosa cells (Figures 2 and 7) [21, 22, 26]; or to the levels of other factors emanating from the *Nr2f2* depleted theca. It is important to note that NR2F2 itself was *not expressed* in granulosa cells of WT or mutant mice with or without DHT and thus the effects of disrupting *Nr2f2* in theca cells on granulosa cells are indirect [21] (Figure 2 and Graphical Abstract). These

results suggest that theca cell NR2F2 is essential for restricting granulosa cell expression of SF1, a key regulator of ovarian functions including steroidogenic genes.

It is also important to note that overexpression of NR5A1/SF1 in SF1 expressing ovarian cells has been shown to lead to altered follicular development and reduced fertility. The ovaries contained polyovular follicles and multiple corpora lutea that expressed steroidogenic genes. In addition, elevated expression of CYP17A1 in specific cells within the stromal compartment was associated with elevated levels of serum testosterone and androstenedione that contributed to a PCOS-like phenotype including obesity in these mice [7].

In 2-month-old *Vcam1* cKO females, transcripts for *Nr2f2*, *Akr1c18*, *Fshr*, and *Runx2* were differentially expressed relative to WT controls (Figure 2). Ovaries of *Vcam1* cKO mice exposed to DHT exhibited specific changes in morphology, downregulated expression of NR2F2 in the theca/stromal compartment, and pMSK1 sampling indicated suppressed proliferation rates in theca and granulosa cells (Figure 5C). Remarkably, this contrasted with the *Nr2f2* cKO + DHT ovaries where the levels of pMSK1 were unimpacted in granulosa cells (Figure 5C). Specifically, DHT treatment of the *Vcam1 cKO* mice increased the expression of CYP11A1 and CYP17A1 in theca cells and induced expression of SF1, CYP11A1, and VCAM1 protein in granulosa cells and some COCs. VCAM1 was also increased markedly in granulosa cells of wild-type mice exposed to exogenous DHT indicating that VCAM1 is not only a target of AR action in theca cells but also in SF1+ granulosa cells. Immuno-HA-tagged LHCGR was increased in theca/stromal cells as well as in some SF1+ granulosa cells of DHT-treated WT mice indicating that AR likely impacts expression of the LHCGR gene as observed in granulosa cells [49] and RNAseq analyses of DHT-treated immature mice [25].

Of note, VCAM1 is essential for early stages of testis development and Leydig cell steroidogenesis but does not appear to be essential for maintaining testis functions in adult mice [48], thus supporting our observations. Likewise, VCAM1 and NR2F2 may regulate early stages of follicle formation but are not essential for later stages that were examined in these experiments by depleting the genes selectively in *Cyp17a1*+ cells.

PCOS phenotype, responses to gonadotropins

Ovaries of women with PCOS contain follicles that are arrested in growth. However, PCOS patients can respond to exogenous hormonal stimulation provided by in vitro fertilization protocols, indicating that there are small follicles contained in ovaries of PCOS women that can be recruited to by-pass mechanisms that disrupt normal follicular growth in these patients and generate functional corpora lutea [3].

The responses of WT and mutant mice to eCG and hCG were distinct. In eCG-treated WT and mutant mice, SF1 was highly expressed in granulosa cells of large antral follicles (Figure 5C); CYP11A1 was elevated in theca and SF1+ stromal cells and in prematurely ovulated/luteinized structures in WT and more strikingly in *Nr2f2* cKO mice but not in the *Vcam1 cKO* mice (Figure 6A–C). In sections from the same ovaries, CYP17A1 was low in theca/stromal cells of eCG-treated WT mice, increased dramatically in theca of the *Vcam1 cKO* mice and intensely stained theca of growing small antral follicles but was absent in luteinizing structures in the *Nr2f2 cKO* (Figure 6A–C). Ovaries of WT, *Vcam1 cKO*, and *Nr2f2 cKO* mice treated with eCG/hCG all contained multiple CYP11A1+ CLs and CYP11A1 positive stromal cells. Sections of these same ovaries exhibited only small, scattered patches of CYP17A1+ stromal cells associated with SF1+ follicles (Supplementary Figure S4).

Expression of patterns of NOTCH1 and INSL3 were also regulated in ovaries of eCG-treated WT and mutant mice, most notably elevated in theca and stromal cells of WT and *Vcam1* cKO mice, but absent in these cells in *Nr2f2 cKO* mouse ovaries that contained numerous CLs where NOTCH1 staining appeared to be associated with vascular elements (Figure 7A–C). INSL3 in these same ovaries was low and notably restricted to CL present in WT mice and TEC and TSC compartments of eCG-treated WT and *Vcam1 cKO* mice. INSL3 was low but co-expressed in SF1+ TEC/TSC in the *Nr2f2* cKO mouse ovary (Figure 7D–F).

In ovaries of WT, *Vcam1 cKO*, and *Nr2f2 cKO* mice treated with eCG + hCG, NOTCH1 co-localized with SF1+ cells within theca and stromal compartments and was notably lower in the *Nr2f2 cKO* ovaries that exhibit a reduced stroma. NOTCH1 also marked vascular elements in the corpora lutea (Supplementary Figure S5). Compared to the expression of CYP11A1 and INSL3 in ovaries of AMC WT and cKO ovaries (Figures 1 and 2), INSL3 was low in CLs present in the eCG–hCG stimulated WT and cKO ovaries, but was present in the SF1 + TSC indicating that these cells might be steroidogenic (Supplementary Figure S5). Expression of INSL3 may be related to the stages of luteinization that occur rapidly in response to the LH surge versus factors that maintain luteal cell function in the cycle or pregnancy. Of relevance, CYP11A1 and INSL3 are elevated in corpora lutea of intact AMC mice (Supplementary Figure S2).

Ovaries of the *Nr2f2* KO mice contained many luteinized-like structures expressing CYP11A1 and SF1+. These features, along with increased ovulation rates in these mice, indicated that ovaries of the *Nr2f2* KO mice were highly sensitive to eCG and hCG leading to enhanced ovulation and normal luteinization. However, the low levels of serum progesterone and the abnormal appearance of the ovaries of the *Nr2f2* mutant mice indicated that the function of the corpora lutea in these mice was restricted/abnormal. Collectively, these results may help explain why the mutant *Nr2f2* mutant mice were subfertile and appeared unable to produce large litters or maintain viable offspring. Furthermore, *NR2F2* has been shown to cooperate with SF1 to regulate the *Insl3* promoter to maintain steroidogenesis in cells in culture [12] and to impact luteal cell maintenance in female mice [50] and testis development in male mice [51].

In addition, expression of 20αHSD (*Akr1c18*) mRNA that converts progesterone [52, 53] to the inactive product trended higher in corpora lutea of the *Nr2f2* mutant mice (Supplementary Figure S2) and may reduce serum progesterone levels in that condition. Thus, the luteal structures may not persist in the mutant mice like those of WT mice where corpora lutea from several cycles reside simultaneously. Reduced expression of *Insl3* may also contribute to this phenotype because *Insl3* mutant mice also exhibit reduced numbers of corpora lutea and were subfertile [50].

Ovaries of *Vcam1* mutant treated with eCG looked similar to those of WT mice. Remarkably, the theca cells of the eCG-treated *Vcam1* cKO mice stained intensely for SF1, CYP11A1, and CYP17A1, indicating enhanced expression of these theca steroidogenic regulatory proteins. In response to

eCG and hCG, the *Vcam1* cKO ovaries contained numerous luteinized-like structures that expressed low levels of SF1 and INSL3 but elevated levels of CYP11A1. Furthermore, the stromal cells were intensely stained for SF1, INSL3, and CYP11A1 indicating that VCAM1 may act to suppress expression of INSL3, possibly by suppressing expression of NR2F2.

Conclusions

The distinct phenotypes of mice in which either *Nr2f2* or *Vcam1* was depleted selectively in theca endocrine cells provide strong evidence that NR2F2 and VCAM1 play key, but distinct, roles in ovarian follicular development, expression of steroidogenic regulatory factors as well as the responses of granulosa cells to elevated levels of androgens (DHT) (see Graphical Abstract) and gonadotropins.

In WT mice treated with DHT, the most notable responses are (1) increased expression of SF1, CYP11A1, CYP17A1, VCAM1, NOTCH1, SF1, and AR in theca endocrine cells and (2) increased expression of SF1, VCAM1, CYP11A1, and LHCGR in granulosa cells.

In the *Nr2f2 cKO* mice, notable features are (1) the loss of stromal cells; (2) abnormal expression of SF1, CYP11A1, VCAM1, and NOTCH1 in granulosa cells of small follicles in response to DHT; (3) decreased expression of NR2F2, CYP11A1, LHCGR, and NOTCH1 in theca cells; (4) increased expression of 20αHSD-associated with "premature" luteinization of granulosa cells in response to eCG and eCG/hCG; and (5) the increased number of ovulated follicles in response to eCG/hCG. Low levels of serum progesterone in adult *Nr2f2* cKO mice and the inability of these mice to sustain pregnancy or nurture young provide additional evidence that NR2F2 depletion in theca cells has profound effects on granulosa cells, follicular development, and luteinization (see Graphical Abstract).

Most notable in the *Vcam1* cKO mice are (1) the enhanced/abnormal expression of SF1, CYP11A1, and VCAM1 and reduced levels of pMSK1 in granulosa cells in response to DHT; (2) enhanced expression of CYP17A1 and INSL3 and decreased expression of NR2F2, CYP11A1, LHCGR, NOTCH1, pMSK1, and 20αHSD in the ovaries following DHT treatment; (3) elevated expression of CYP17A1 in theca cells of large antral follicles in response to eCG; and (4) ovulation in response to eCG/hCG despite lower relative levels of progesterone in mature *Vcam1* cKO mice.

These results provide notable clues that may help explain not only the anovulatory phenotype observed women with PCOS who have (1) elevated ovarian androgen levels and follicles that undergo premature growth arrest; (2) altered expression of theca cell genes, including NR2F2, NR4A1, AR, INSL3, and VCAM1 [16, 21, 22, 25, 26]; potentially reduced expression of follicular NOTCH1 [54] but who are (3) capable of ovulating in response to exogenous gonadotropin treatments.

Acknowledgment

We thank colleagues at Baylor College of Medicine, Dr Fabio Stossi and Hannah Johnson in the Integrated Microscopy Core and Patricia Castro in the Pathology and Histology Core, for their assistance and advice.

Supplementary material

Supplementary material is available at *BIOLRE* online.

Author contributions

NRC planned, performed, and carried out all experiments presented in this manuscript, and wrote the results, figure legends, and materials section, which were further edited by JSR. JSR determined experimental direction of the manuscript and wrote the introduction, discussion, and abstract sections.

Conflict of Interest

The authors have declared that no conflict of interest exists.

Data availability

Higher resolution versions of the figures (and individual images) in this manuscript are available upon request.

References

1. Diamanti-Kandarakis E, Dunaif A. Insulin resistance and the polycystic ovary syndrome revisited: an update on mechanisms and implications. *Endocr Rev* 2012; **33**:981–1030.
2. Dumesic DA, Richards JS. Ontogeny of the ovary in polycystic ovary syndrome. *Fertil Steril* 2013; **100**:23–38.
3. Adams J, Liu Z, Ren YA, Wun W-S, Zhou W, Kenigsberg S, Librach C, Valdes C, Gibbons W, Richards J. Enhanced inflammatory transcriptome in the granulosa cells of women with polycystic ovarian syndrome. *J Clin Endocrinol Metab* 2016; **101**:3459–3468.
4. Rosenfield RL, Ehrmann DA. The pathogenesis of polycystic ovary syndrome (PCOS): the hypothesis of PCOS as functional ovarian hyperandrogenism revisited. *Endocr Rev* 2016; **37**:467–520.
5. Dapas M, Dunaif A. The contribution of rare genetic variants to the pathogenesis of polycystic ovary syndrome. *Curr Opin Endocr Metab Res* 2020; **12**:26–32.
6. McAllister JM, Modi B, Miller BA, Biegler J, Bruggeman R, Legro RS, Strauss JF. Overexpression of a DENND1A isoform produces a polycystic ovary syndrome theca phenotype. *Proc Natl Acad Sci U S A* 2014; **111**:5455–5455.
7. Rotgers E, Nicol B, Rodriguez K, Rattan S, Flaws JA, Yao HHC. Constitutive expression of steroidogenic factor-1 (NR5A1) disrupts ovarian functions, fertility, and metabolic homeostasis in female mice. *FASEB J* 2021; **35**:e21770-n/a.
8. Richards JS, Sharma SC, Falender AE, Lo YH. Expression of FKHR, FKHRL1, and AFX genes in the rodent ovary: evidence for regulation by IGF-I, estrogen, and the gonadotropins. *Mol Endocrinol* 2002; **16**:580–599.
9. Nomura R, Kashimada K, Suzuki H, Zhao L, Tsuji-Hosokawa A, Yagita H, Takagi M, Kanai Y, Bowles J, Koopman P, Kanai-Azuma M, Morio T. Nr5a1 suppression during the murine fetal period optimizes ovarian development by fine-tuning notch signaling. *J Cell Sci* 2019; **132**:jcs223768.
10. Pierson, Smela MD, Kramme CC, Fortuna PRJ, Adams JL, Su R, Dong E, Kobayashi M, Brixi G, Kavirayuni VS, Tysinger E, Kohman RE, Shioda T, *et al.* Directed differentiation of human iPSCs to functional ovarian granulosa-like cells via transcription factor overexpression. *Elife* 2023; **12**:e83291.
11. Parker KL, Schimmer BP. Steroidogenic factor 1: a key determinant of endocrine development and function. *Endocr Rev* 1997; **18**:361–377.
12. Mendoza-Villarroel RE, Di-Luoffo M, Camiré E, Giner XC, Brousseau C, Tremblay JJ. The INSL3 gene is a direct target for the orphan nuclear receptor, COUP-TFII, in Leydig cells. *J Mol Endocrinol* 2014; **53**:43–55.

13. de Mattos K, Viger RS, Tremblay JJ. Transcription factors in the regulation of Leydig cell gene expression and function. *Front Endocrinol (Lausanne)* 2022; **13**:881309–881309.
14. Mehanovic S, Mendoza-Villarroel RE, de Mattos K, Talbot P, Viger RS, Tremblay JJ. Identification of novel genes and pathways regulated by the orphan nuclear receptor COUP-TFII in mouse MA-10 Leydig cells. *Biol Reprod* 2021; **105**:1283–1306.
15. Ivell R, Alhujaili W, Kohsaka T, Anand-Ivell R. Physiology and evolution of the INSL3/RXFP2 hormone/receptor system in higher vertebrates. *Gen Comp Endocrinol* 2020; **299**: 113583–113594.
16. Dai Y, Ivell R, Anand-Ivell R. Theca cell INSL3 and steroids together orchestrate the growing bovine antral follicle. *Front Physiol* 2017; **8**:1–14.
17. Satchell L, Glister C, Bleach EC, Glencross RG, Bicknell AB, Dai Y, Anand-Ivell R, Ivell R, Knight PG. Ovarian expression of insulin-like peptide 3 (INSL3) and its receptor (RXFP2) during development of bovine antral follicles and corpora lutea and measurement of circulating INSL3 levels during synchronized estrous cycles. *Endocrinology (Philadelphia)* 2013; **154**:1897–1906.
18. Glister C, Satchell L, Bathgate RAD, Wade JD, Dai Y, Ivell R, Anand-Ivell R, Rodgers RJ, Knight PG. Functional link between bone morphogenetic proteins and insulin-like peptide 3 signaling in modulating ovarian androgen production. *Proc Natl Acad Sci U S A* 2013; **110**:E1426–E1435.
19. Saddick SY. Identifying genes associated with the development of human polycystic ovary syndrome. *Saudi J Biol Sci* 2020; **27**: 1271–1279.
20. Xue K, Liu J-y, Murphy BD, Tsang BK. Orphan nuclear receptor NR4A1 is a negative regulator of DHT-induced rat preantral follicular growth. *Mol Endocrinol* 2012; **26**:2004–2015.
21. Li M, Xue K, Ling J, Diao F-Y, Cui Y-G, Liu J-Y. The orphan nuclear receptor NR4A1 regulates transcription of key steroidogenic enzymes in ovarian theca cells. *Mol Cell Endocrinol* 2010; **319**:39–46.
22. Dai A, Yan G, He Q, Jiang Y, Zhang Q, Fang T, Ding L, Sun J, Sun H, Hu Y. Orphan nuclear receptor Nur77 regulates androgen receptor gene expression in mouse ovary. *PloS One* 2012; **7**:e39950–e39950.
23. Richards JS, Ren YA, Candelaria N, Adams JE, Rajkovic A. Ovarian follicular theca cell recruitment, differentiation, and impact on fertility: 2017 update. *Endocr Rev* 2018; **39**:1–20.
24. Lee S, Kang D-W, Hudgins-Spivey S, Krust A, Lee E-Y, Koo Y, Cheon Y, Gye MC, Chambon P, Ko C. Theca-specific estrogen receptor-α knockout mice lose fertility prematurely. *Endocrinology (Philadelphia)*. 2009; **150**:3855–3862.
25. Candelaria NR, Padmanabhan A, Stossi F, Ljungberg MC, Shelly KE, Pew BK, Solis M, Rossano AM, McAllister JM, Wu S, Richards JS. VCAM1 is induced in ovarian theca and stromal cells in a mouse model of androgen excess. *Endocrinology* 2019; **160**: 1377–1393.
26. Song J, Diao F, Ma X, Xu S, Cui Y, Jiang S, Liu J. Androgen upregulates NR4A1 via the TFAP2A and ETS signaling networks. *Int J Biochem Cell Biol* 2019; **113**:1–7.
27. Ma Y, Andrisse S, Chen Y, Childress S, Xue P, Wang Z, Jones D, Ko C, Divall S, Wu S. Androgen receptor in the ovary theca cells plays a critical role in androgen-induced reproductive dysfunction. *Endocrinology (Philadelphia)* 2017; **158**:98–108.
28. Osborn L, Hession C, Tizard R, Vassallo C, Luhowskyj S, Chi-Rosso G, Lobb R. Direct expression cloning of vascular cell adhesion molecule 1, a cytokine-induced endothelial protein that binds to lymphocytes. *Cell* 1989; **59**:1203–1211.
29. Hu X-L, Chen G, Zhang S, Zheng J, Wu J, Bai Q-R, Wang Y, Li J, Wang H, Feng H, Li J, Sun X, *et al*. Persistent expression of VCAM1 in radial glial cells is required for the embryonic origin of postnatal neural stem cells. *Neuron (Cambridge, Mass)* 2017; **95**:309–325.e6.
30. Gurtner GC, Davis V, Li H, McCoy MJ, Sharpe A, Cybulsky MI. Targeted disruption of the murine VCAM1 gene: essential role of VCAM-1 in chorioallantoic fusion and placentation. *Genes Dev* 1995; **9**:1–14.
31. Takamoto N, Kurihara I, Lee K, DeMayo FJ, Tsai M-J, Tsai SY. Haploinsufficiency of chicken ovalbumin upstream promoter transcription factor II in female reproduction. *Mol Endocrinol* 2005; **19**:2299–2308.
32. Tsai SY, Tsai MJ. Chick ovalbumin upstream promoter-transcription factors (COUP-TFs): coming of age. *Endocr Rev* 1997; **18**:229–240.
33. Petit FG, Jamin SP, Kurihara I, Behringer RR, DeMayo FJ, Tsai M-J, Tsai SY. Deletion of the orphan nuclear receptor COUP-TFII in uterus leads to placental deficiency. *Proc Natl Acad Sci U S A* 2007; **104**:6293–6298.
34. Koni P, Joshi SK, Temann U, Olson D, Burkly L, Flavell R. Conditional vascular cell adhesion molecule 1 deletion in mice: impaired lymphocyte migration to bone marrow. *J Exp Med* 2001; **193**:741–754.
35. Bridges PJ, Koo Y, Kang D-W, Hudgins-Spivey S, Lan Z-J, Xu X, DeMayo F, Cooney A, Ko C. Generation of Cyp17iCre transgenic mice and their application to conditionally delete estrogen receptor alpha (Esr1) from the ovary and testis. *Genesis*(New York, NY: 2000) 2008; **46**:499–505.
36. Nelson VL, Legro RS, S, MA. Augmented androgen production is a stable steroidogenic phenotype of propagated theca cells from polycystic ovaries. *Mol Endocrinol* 1999; **13**:946–957.
37. Baena V, Owen CM, Uliasz TF, Lowther KM, Yee S-P, Terasaki M, Egbert JR, Jaffe LA. Cellular heterogeneity of the luteinizing hormone receptor and its significance for cyclic GMP signaling in mouse preovulatory follicles. *Endocrinology (Philadelphia)* 2020; **161**:1.
38. Liu C, Peng J, Matzuk MM, Yao HHC. Lineage specification of ovarian theca cells requires multicellular interactions via oocyte and granulosa cells. *Nat Commun* 2015; **6**:6934–6945.
39. Koike H, Harada M, Kusamoto A, Kunitomi C, Xu Z, Tanaka T, Urata Y, Nose E, Takahashi N, Wada-Hiraike O, Hirota Y, Koga K, *et al*. Notch signaling induced by endoplasmic reticulum stress regulates cumulus-oocyte complex expansion in polycystic ovary syndrome. *Biomolecules* 2022; **12**:1037.
40. Zhang C-P, Yang J-L, Zhang J, Li L, Huang L, Ji S-Y, Hu Z-Y, Gao F, Liu Y-X. Notch signaling is involved in ovarian follicle development by regulating granulosa cell proliferation. *Endocrinology* 2011; **152**:2437–2447.
41. Vanorny DA, Prasasya RD, Chalpe AJ, Kilen SM, Mayo KE. Notch signaling regulates ovarian follicle formation and coordinates follicular growth. *Mol Endocrinol* 2014; **28**:499–511.
42. Prasasya RD, Mayo KE. Notch signaling regulates differentiation and steroidogenesis in female mouse ovarian granulosa cells. *Endocrinology* 2018; **159**:184–198.
43. Hubbard N, Prasasya RD, Mayo KE. Activation of notch signaling by oocytes and Jag1 in mouse ovarian granulosa cells. *Endocrinology* 2019; **160**:2863–2876.
44. Garton KJ, Gough PJ, Philalay J, Wille PT, Blobel CP, Whitehead RH, Dempsey PJ, Raines EW. Stimulated shedding of vascular cell adhesion molecule 1 (VCAM-1) is mediated by tumor necrosis factor-α-converting enzyme (ADAM 17). *J Biol Chem* 2003; **278**: 37459–37464.
45. Richards JS, Fitzpatrick SL, Clemens JW, Morris JK, Alliston T, Sirois J. Ovarian cell differentiation: a cascade of multiple hormones, cellular signals, and regulated genes. *Recent Prog Horm Res* 1995; **50**:223–254.
46. Richards JS, Pangas SA. The ovary: basic biology and clinical implications. *J Clin Invest* 2010; **120**:963–972.
47. Richards JS, Candelaria NR, Lanz RB. Polyploid giant cancer cells and ovarian cancer: new insights into mitotic regulators and polyploidy. *Biol Reprod* 2021; **105**:305–316.
48. Karpova T, Ravichandiran K, Insisienmay L, Rice D, Agbor V, Heckert LL. Steroidogenic factor 1 differentially regulates fetal and adult Leydig cell development in male mice. *Biol Reprod* 2015; **93**: 1–15.

49. Richards JS. Hormonal control of gene expression in the ovary. *Endocr Rev* 1994; **15**:725–751.
50. Spanel-Borowski K, Schäfer I, Zimmermann S, Engel W, Adham IM. Increase in final stages of follicular atresia and premature decay of corpora lutea in Insl3-deficient mice. *Mol Reprod Dev* 2001; **58**: 281–286.
51. Zimmermann S, Steding G, Emmen JMA, Brinkmann AO, Nayernia K, Holstein AF, Engel W, Adham IM. Targeted disruption of the Insl3 gene causes bilateral cryptorchidism. *Mol Endocrinol* 1999; **13**:681–691.
52. Akinola LA, Poutanen M, Vihko R, Vihko P. Expression of 17β-hydroxysteroid dehydrogenase type 1 and type 2, P450 aromatase, and 20α-hydroxysteroid dehydrogenase enzymes in immature, mature, and pregnant rats∗. *Endocrinology* 1997; **138**: 2886–2892.
53. Stocco C, Telleria C, Gibori G. The molecular control of corpus luteum formation, function, and regression. *Endocr Rev* 2007; **28**: 117–149.
54. Moldovan GE, Miele L, Fazleabas AT. Notch signaling in reproduction. *Trends Endocrinol Metab* 2021; **32**:1044–1057.